Petroleum Science 23 (2026) 4488–4504

Contents lists available at ScienceDirect

Petroleum Science

journal homepage: www.keaipublishing.com/en/journals/petroleum-science

Original Paper

Occurrence characterizations and controlling factors of lacustrine shale pore fluids in the Qingshankou Formation, Sanzhao Sag, Songliao Basin, China

Jun-Hui Li [a,b], Fang-Ju Chen [a,b], Jie Li [a,b], Peng-Fei Zhang [c,*], Yan-Ping Zhu [a,b], Neng-Wu Zhou [c], Jia-Wei Hao [a,b], Wei-Zheng Gao [c], Shuang-Fang Lu [c,**]

[a] State Key Laboratory of Continental Shale Oil, Daqing, 163712, Heilongjiang, China
[b] Exploration and Development Research Institute of PetroChina Daqing Oilfield Company Limited, Daqing, 163712, Heilongjiang, China
[c] Sanya Offshore Oil & Gas Research Institute of Northeast Petroleum University, Sanya, 572025, Hainan, China

ARTICLE INFO

Article history:
Received 22 January 2025
Received in revised form
12 December 2025
Accepted 4 June 2026
Available online 10 June 2026

Edited by Xiu-Fang Hu

Keywords:
Occurrence characterization
Pore structure
Nuclear magnetic resonance
Shale oil
Sanzhao Sag
Songliao Basin

ABSTRACT

The pore fluid occurrence predominantly restricts shale oil production. Few studies have addressed both pore oil and water concurrently. In an effort to delineate the distribution of pore fluids within shale oil reservoirs, this study collected diverse shale samples from the Qingshankou Formation in the Sanzhao Sag, Songliao Basin, China. The in-situ pore fluids were initially resurrected under equilibrium moisture conditions and subsequently saturated with light oil. A comprehensive suite of analytical techniques was employed in tandem, encompassing total organic carbon (TOC), Rock-Eval, X-ray diffraction (XRD), scanning electron microscopy (SEM), low-temperature nitrogen adsorption-desorption, and nuclear magnetic resonance (NMR). The occurrence characterizations of pore fluids were clarified by NMR T_1–T_2 spectra across various states, shedding light on the governing factors. A pattern of pore-fluid occurrence in shale oil reservoirs was proposed. Results indicate that NMR T_1–T_2 combined with water and oil restoration effectively assesses the distribution of in-situ pore fluids. Capillary-bound water primarily contributes to pore fluids, with nearly half being depleted at the as-received state. Shale oil mainly comprises capillary-bound oil, succeeded by adsorbed and movable oil. The alterations in shale oil occurrence characteristics are synchronous with the depletion of pore fluids. NMR T_1–T_2 primarily detects the adsorbed oil in shale pores, whereas Rock-Eval is capable of quantifying oil adsorbed on pore surfaces and absorbed within organic matter. NMR T_1–T_2 offers a more precise technique for quantitatively evaluating shale pore fluids. Micropores (<25 nm) and minipores (25–100 nm) are primarily saturated with capillary-bound water, accompanied by a minor fraction of adsorbed oil. Capillary-bound and movable oil are primarily distributed within mesopores (100–1000 nm) and macropores (>1000 nm), respectively. Consequently, adsorbed oil is significantly influenced by pore water, followed by capillary-bound oil, while movable oil remains largely unaffected. Felsic-rich (FR) shales may represent the optimal lithology for shale oil enrichment, characterized by the development of interparticle pores, a lower Brunauer-Emmett-Teller (BET) specific surface area, and abundant meso- and macropores. These insights into the characteristics of pore fluids in shale oil reservoirs could bolster shale oil exploration in the Sanzhao Sag.

1. Introduction

A cascade of successful ventures in shale oil exploration and development has positioned it as a viable alternative to traditional oil and gas resources, intensifying the so-called “shale revolution” (Zhao et al., 2023a; Jia et al., 2024; Li et al., 2024a; Wang et al., 2025a). Recently, significant breakthroughs have been achieved in lacustrine shale oil in Chna (Jin et al., 2022). Shale oil has been

* Corresponding author.
** Corresponding author.
E-mail addresses: zhangpengfei@nepu.edu.cn (P.-F. Zhang), lushuangfang@nepu.edu.cn (S.-F. Lu).
Peer review under the responsibility of China University of Petroleum (Beijing).

https://doi.org/10.1016/j.petsci.2026.06.008

developed in multiple strata, such as the Qingshankou Formation in the Gulong Sag (Zhang et al., 2023a; Zhao et al., 2023b), the Shahejie Formation in the Bohai Bay Basin (Liu et al., 2022a; Zhao et al., 2023c), the Luchaogou Formation in the Jimsar Sag (Cao et al., 2023, 2024), and the Funing Formation in the Subei Basin (Fang et al., 2023; Zhu et al., 2023). However, shale oil production exhibits considerable variation across these strata (Gao et al., 2024). The occurrence characterizations of pore fluids have emerged as a pivotal determinant in the efficient exploitation of shale oil, garnering progressively escalating attention within the industry (Dang et al., 2022; Li et al., 2022a; Tian et al., 2024).

Previous studies have provided a range of techniques and methods for analyzing the occurrence of pore fluids in shale oil reservoirs (Hu et al., 2021; Wang et al., 2022a; Xu et al., 2022). Rock-Eval is recognized as the most prevalent and convenient technique for such analyses. It allows for the calculation of total, adsorbed, and free oil by comparing Rock-Eval parameters before and after an oil-washed process (Jarvie, 2012; Bai et al., 2022), which can also be directly assessed through the multi-stage Rock-Eval method (Jiang et al., 2016). Furthermore, multi-step extraction has been developed to explore the contents and occurrence pore sizes of shale oil in different states combined with low-temperature nitrogen adsorption-desorption (LTNA/D) and mercury intrusion capillary pressure (MICP) (Su et al., 2018; Wang et al., 2019; Zhang et al., 2019a). Molecular dynamics simulation is considered the optimal approach for disclosing the micro-occurrence characterizations of shale oil, providing clarity on the thickness and density of adsorbed oil (Tian et al., 2018; Yang et al., 2020; Wang et al., 2025b). Recently, a series of theoretical models have been devised to describe shale pore fluid distributions (Li et al., 2017, 2018a). Combined with centrifugal or thermogravimetric analyses, the features of adsorbed oil in shales, i.e., average thickness and density, are defined by the adsorption ratio equation (Zhang et al., 2022a, 2023b). Adsorbed and free oil are then calculated based on the pore size distribution (PSD) of shale (Zhang et al., 2023b).

However, the methods under discussion predominantly concentrate on oil within shale pore networks or in a state of saturation, often overlooking the presence of pore water. Previous studies have primarily focused on pore water in gas shales, i.e., shale gas reservoirs with high or over-maturity, due to the profound influence of pore water on the content and occurrence of shale gas (Cheng et al., 2022; Ma and Yu, 2022; Li et al., 2024b). Similarly, shale oil can also be severely affected by pore water (Li et al., 2024c). Actually, a large amount of pore water generally occurs in shale oil reservoirs with relatively low maturity (Wang et al., 2025c). Therefore, paying greater heed to the role of pore water is imperative. NMR T_1–T_2 provides an innovation for simultaneously detecting multiphase fluids in shale pore systems (Li et al., 2018b; Liu et al., 2022b; Wang et al., 2025c). T_1–T_2 spectra, derived from preserved shale samples, are adept at assessing the distribution and quantity of both pore oil and water, showing a high degree of correlation with the Dean-Stark extraction technique (Li et al., 2022a). Unfortunately, preserved shale samples are seldom available, whereas as-received shale samples are ubiquitous and often characterized by a depletion of pore fluids (Li et al., 2022a). It is essential to account for and restore the lost pore water and oil to reflect the state of in-situ pore fluids accurately.

The occurrence of pore fluids in shales is governed by a multitude of factors, including organic matter, mineral composition, pore structure, etc. (Jarvie, 2012; Wang et al., 2015, 2022b). Shale oil is inherently linked to organic matter, with higher organic content typically correlating with a greater shale oil content (Wang et al., 2015). The wettability of minerals controls the micro-distributions of pore fluids in shales (Xue et al., 2022). Pore water and oil are closely related to pore structures, with a higher prevalence of larger pores and simpler structures conducive to shale oil accumulation, particularly free oil (Zhang et al., 2023b). However, pore water has often been overlooked. Moreover, the controlling factors of pore fluids in shale full-scale PSD should be taken seriously.

The Sanzhao Sag is located in the Central Depression of the Songliao Basin. The Qingshankou Formation is the primary source rock with a high organic matter content, characterized by a lower maturity than that in the Gulong Sag (Zhang et al., 2023a). The Qingshankou Formation in the Sanzhao Sag is also an exploration target for shale oil in the Songliao Basin. However, few studies have focused on the occurrence of pore fluids in shales. Thus, this study aims to explore pore-fluid distribution in shale oil reservoirs and the controlling factors in the Sanzhao Sag. As per previous studies (Zhang et al., 2024a, 2024b), the in-situ shale pore fluids were first reconstructed by absorbing water and saturated light oil. Meanwhile, a range of tests were conducted on the shales from the Qingshankou Formation, including total organic carbon (TOC), Rock-Eval, X-ray diffraction (XRD), scanning electron microscopy (SEM), LTNA/D, and NMR. A pattern of pore-fluid occurrence in shale oil reservoirs was developed. This study offers an in-depth understanding of the occurrence characteristics of pore fluids in shale oil reservoirs, which is instrumental for exploring and developing shale oil resources in the Sanzhao Sag.

2. Methodology

2.1. Samples

This study collected 22 shale samples from the Qingshankou Formation in the Sanzhao Sag, Songliao Basin, Northeast China. The Qingshankou Formation was deposited in the semi-deep to deep lake environment with freshwater to brackish water (Bechtel et al., 2012; Wang et al., 2023; Wu et al., 2024). It is the main source rock and the primary shale oil exploration target in the Songliao Basin. In this study, 13 shales were sampled from the First Member of the Qingshankou Formation (K_1nq^1), while the others were derived from the Second and Third Members (K_1nq^{2+3}). All shales were cut using the wire-cutting technique under anhydrous conditions to obtain the core plugs with diameters of about 25 mm and lengths ranging from 30 mm to 50 mm. The core cuttings were crushed into powder. NMR measurements were conducted on the core plugs, and the powders were used to perform TOC, Rock-Eval, XRD, and LTNA/D. Furthermore, SEM images were obtained from the core cuttings after polishing with argon particles.

2.2. Experiments

2.2.1. SEM and LTNA/D tests

Prior to the SEM tests, the core cuttings were first cleaned to remove residual oil using a mixed solution of dichloromethane and acetone (3:1 in volume) under a temperature of 85 °C and a pressure of 0.25 MPa for 14 d. Then, samples were dried at 110 °C for 24 h under vacuum conditions. The cuttings were first manually polished and then polished with argon particles to obtain a flat surface. A series of SEM images were collected from a Phenom ProX scanning electron microscope at a maximum magnification of 12,000×.

LTNA/D experiments were performed on a Micromeritics ASAP 2460 surface area and porosity analyzer. Before the tests, the core cuttings were crushed into powders (40–60 mesh), and then cleaned and dried using the same method. Nitrogen adsorption and desorption isotherms were collected at relation pressure (P/P_0) between 0.01 and 0.993 at 77 K. The specific surface area (SSA)

was calculated by the BET model. This study adopted the pore classification scheme of micropores (<25 nm), minipores (25–100 nm), mesopores (100–1000 nm), and macropores (>1000 nm) (Zhang et al., 2017).

2.2.2. NMR tests

NMR experiments were conducted on five states: as-received (AR), water restoration (WR), water and oil restoration (WOR), oil-washed and dried (Dry), and oil-saturated (SO) (Zhang et al., 2024a, 2024b). The AR state refers to shale samples without any treatments after cutting. The loss of pore fluids is severe due to changes in temperature and pressure (Li et al., 2022a, 2022b). To restore the in-situ pore water, the AR shales were placed in a high relative humidity environment (RH ≈ 0.98). During this process, the sample mass was recorded every 12 h. When the difference in sample mass between two consecutive measurements is less than 0.0005 g, it is considered that water recovery is complete, and the state is marked as WR. Subsequently, the WR shales were saturated with light oil (n-dodecane, in this study) for 24 h using a vacuum pressure saturator, after vacuuming for 1 h to restore the lost light oil, which is recognized as the WOR state. It may not be possible to minimize evaporation of pore water during oil saturation when the vacuum pumping time is reduced to 1 h. Shale samples were then oil-washed using the same method as discussed in Section 2.2.1, and dried under vacuum (pressure less than −0.1 MPa) for 24 h to obtain the Dry state. Finally, the dry shales were saturated with *n*-dodecane for 24 h using a vacuum-pressure saturator after vacuuming for 6 h, resulting in the SO state.

NMR tests were carried out on a MesoMR12-060H-I NMR spectrometer (Niumag, Suzhou, China) with a resonance frequency of about 12 MHz and a low magnetic field of 0.3 ± 0.05 T. The CPMG and SR-CPMG sequences were employed to detect T_2 and T_1–T_2 spectra, respectively. The test parameters were set as follows: TW = 3000 ms, TE = 0.07 ms, NS = 32, NECH = 8192, and NTI = 31. The extremely low TE value is conducive to detecting the nanopores in shale oil reservoirs.

3. Results and discussion

3.1. Organic geochemistry and mineral compositions of shales

TOC, S_1, S_2, and T_{max} of the studied samples are detailed in Table 1. TOC has a large average value of 3.55%, ranging from 0.35% to 9.67%, and the samples from the First Member are generally characterized by higher TOC contents (mean 4.28%) than the shales from the Second and Third Members of the Qingshankou Formation (mean 2.26%). Correspondingly, a large average S_1 value of 2.91 mg/g is observed, spanning from 0.53 mg/g to 7.58 mg/g, while S_2 is between 0.80 mg/g and 42.99 mg/g, with a mean of 18.10 mg/g, which is mainly larger than that of the Qingshankou Formation in the Gulong Sag, Songliao Basin (Bai et al., 2022; Zhang et al., 2023c). T_{max} varies from 438 °C to 450 °C (mean 445 °C), indicating a low-maturity to maturity. As a result, the studied shales are predominantly in the low to mature stage, which correlates with higher S_2 values compared to those in the Qingshankou Formation in the Gulong Sag.

The mineral composition of the selected shales is predominantly quartz, clay minerals, and feldspar, as illustrated in Fig. 1(a). Quartz averages 28.8%, with a range of 10.8% to 46.8%, and clay minerals span from 2.8% to 44.4%, with a mean of 26.9%. Feldspar has an average of 18.9%, ranging from 1.4% to 37.1%. Moreover, elevated concentrations of dolomite are detected in certain shales, with the maximum content reaching 77.2%, and the same goes for calcite, characterized by the largest value of 79.5%. A minor presence of orthoclase is also noted, averaging at 2.6% (1.7%–3.4%). In comparison to the shales from the Qingshankou Formation in the Gulong Sag (Liu et al., 2018), the studied shales in the Sanzhao Sag exhibit a higher content of carbonate minerals but a lower abundance of felsic minerals, particularly feldspar.

Table 1
TOC and conventional Rock-Eval parameters of the selected shales.

Samples	Depth, m	Formation	TOC, %	S_1, mg/g	S_2, mg/g	T_{max}, °C
ZY1-1	1931.20	K_1qn^{2+3}	0.35	0.53	0.80	438
ZY1-2	1932.00	K_1qn^{2+3}	3.32	2.14	18.68	447
ZY1-3	1935.50	K_1qn^{2+3}	2.03	1.64	11.16	446
ZY1-5	1941.90	K_1qn^{2+3}	5.20	3.13	29.00	448
ZY1-6	1955.30	K_1qn^{2+3}	2.70	2.08	14.92	446
ZY1-7	1958.10	K_1qn^{2+3}	1.93	2.14	9.95	441
ZY1-8	1958.90	K_1qn^{2+3}	1.10	1.18	5.33	439
ZY1-9	1961.90	K_1qn^{2+3}	1.47	1.21	8.84	444
ZY1-10	1972.21	K_1qn^1	4.32	2.49	25.50	447
ZY1-11	1980.95	K_1qn^1	3.97	2.31	19.40	441
ZY1-12	1987.40	K_1qn^1	6.02	3.52	34.53	450
ZY1-13	1993.30	K_1qn^1	5.74	3.70	29.12	447
ZY1-14	1997.87	K_1qn^1	2.52	2.62	12.81	443
ZY1-16	2005.44	K_1qn^1	3.06	3.05	14.44	447
ZY1-17	2010.34	K_1qn^1	2.99	1.83	16.41	449
ZY1-18	2016.54	K_1qn^1	5.19	2.50	31.45	450
ZY1-19	2024.35	K_1qn^1	3.58	3.51	16.60	445
ZY1-20	2027.80	K_1qn^1	9.67	7.58	42.99	439
ZY1-21	2037.75	K_1qn^1	2.87	2.69	10.24	438
ZY1-22	2039.52	K_1qn^1	4.60	6.90	24.19	449
ZY1-23	2043.84	K_1qn^1	3.04	4.08	12.64	440
ZY1-24	2049.77	K_1qn^1	2.32	3.12	9.27	448

Therefore, the selected shales in the Sanzhao Sag are characterized by lower maturity and more carbonate minerals but less feldspar when juxtaposed with those in the Gulong Sag. However, the selected shales in the Sanzhao Sag have much lower carbonate content than those from the Shahejie Formation in the Jiyang Depression (Su et al., 2018, 2019), suggesting that the studied shales formed mainly in freshwater to brackish-water environments. Lithology is considered an indicator of sweet spots in shale oil and gas (Jiang et al., 2026). A classification scheme has been adopted, as shown in Fig. 1(b) (Fang et al., 2023; Zhu et al., 2023). Specifically, the selected shales primarily belong to clay-bearing calcareous felsic-rich (CBCFR) shales, followed by felsic-rich (FR), calcareous-rich (CR), and felsic-calcareous mixed (FCM) shales.

3.2. Shale oil contents derived from Rock-Eval

Multi-stage Rock-Eval is a proven methodology for the detection of shale oil in various states, including adsorbed and free oil (Jiang et al., 2016). As displayed in Table 2, the values of $S_{1\text{-}1}$ (light oil) are low, with a mean of 0.13 mg/g (0.02–0.24 mg/g), meaning that most of the light oil in shales is lost. The light to medium oil, i.e., $S_{1\text{-}2}$, is between 0.41 and 7.90 mg/g, with an average of 3.33 mg/g. Correspondingly, the free oil ($S_{1\text{-}1}$+$S_{1\text{-}2}$) ranges from 0.43 mg/g to 8.13 mg/g, with a mean of 3.45 mg/g. However, the adsorbed oil ($S_{2\text{-}1}$) varies from 0.59 mg/g to 30.88 mg/g, with a large average of 10.48 mg/g. As a result, the total oil is between 1.02 mg/g and 39.01 mg/g (mean 13.93 mg/g). Notably, lower maturity levels are associated with a higher proportion of adsorbed oil compared to those observed in the Gulong Sag (Zhang et al., 2023c, 2024b).

The relationships of S_1 with free and total oil are plotted in Fig. 2(a). An excellent correlation is observed between S_1 and free oil, allowing for the determination of the free oil correction coefficient for S_1 (k_f), with a value of about 1.16. This value is lower than that derived from liquid-nitrogen-frozen shales from the

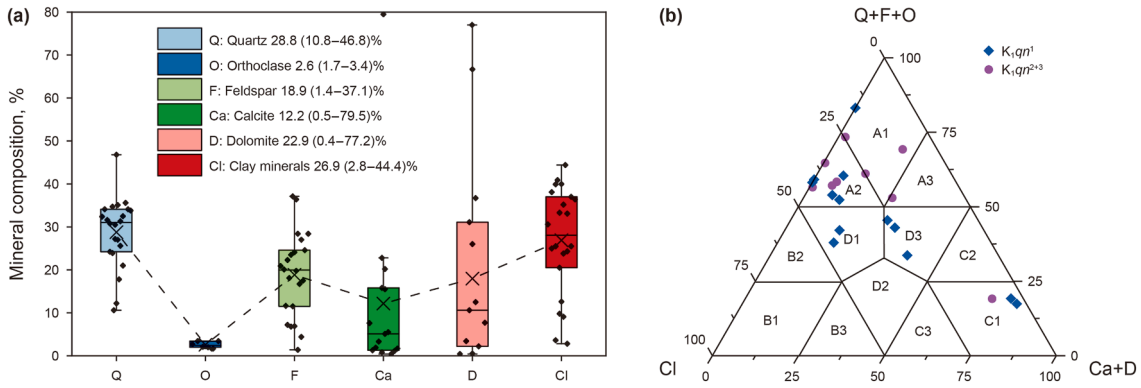

Fig. 1. Mineral compositions **(a)** and lithologies **(b)** of the studied shales (Fang et al., 2023; Zhu et al., 2023). A1, A2, and A3 are the felsic-rich (FR), carbonate-bearing argillaceous felsic-rich (CBAFR), and clay-bearing calcareous felsic-rich (CBCFR) shales; B1, B2, and B3 represent the argillaceous-rich (AR), carbonate-bearing felsic argillaceous-rich (CBFAR), and felsic-bearing calcareous argillaceous-rich (FBCAR) shales; C1, C2, and C3 refer to calcareous-rich (CR), clay-bearing felsic calcareous-rich (CBFCR), and felsic-bearing argillaceous calcareous-rich (FBACR) shales; D1, D2, and D3 are felsic-argillaceous mixed (FAM), argillaceous-calcareous mixed (ACM), and felsic-calcareous mixed (FCM) shales.

Table 2
Multi-stage Rock-Eval parameters of the studied shales.

Samples	Depth, m	$S_{1\text{-}1}$, mg/g	$S_{1\text{-}2}$, mg/g	$S_{2\text{-}1}$, mg/g	$S_{2\text{-}2}$, mg/g	Free oil, mg/g	Total oil, mg/g
ZY1-1	1931.20	0.02	0.41	0.59	0.19	0.43	1.02
ZY1-2	1932.00	0.08	2.57	10.48	8.65	2.65	13.14
ZY1-3	1935.50	0.07	2.03	6.57	4.13	2.10	8.67
ZY1-5	1941.90	0.19	3.08	14.93	12.42	3.26	18.20
ZY1-6	1955.30	0.10	2.66	8.96	5.84	2.76	11.72
ZY1-7	1958.10	0.07	2.47	6.70	2.71	2.54	9.25
ZY1-8	1958.90	0.07	1.55	3.78	1.22	1.62	5.40
ZY1-9	1961.90	0.07	1.50	5.60	2.70	1.57	7.17
ZY1-10	1972.21	0.09	2.71	14.51	10.82	2.80	17.31
ZY1-11	1980.95	0.08	3.49	12.98	7.46	3.57	16.55
ZY1-12	1987.40	0.22	4.12	16.51	17.45	4.35	20.85
ZY1-13	1993.30	0.20	3.89	15.94	12.86	4.09	20.02
ZY1-14	1997.87	0.24	2.87	7.95	4.69	3.11	11.06
ZY1-16	2005.44	0.17	3.90	8.08	5.47	4.07	12.15
ZY1-17	2010.34	0.13	2.05	8.43	7.78	2.17	10.60
ZY1-18	2016.54	0.15	3.01	15.09	16.02	3.16	18.25
ZY1-19	2024.35	0.17	4.03	9.74	6.18	4.19	13.93
ZY1-20	2027.80	0.22	7.90	30.88	11.69	8.13	39.01
ZY1-21	2037.75	0.08	2.79	6.54	2.78	2.87	9.41
ZY1-22	2039.52	0.21	7.26	12.71	9.81	7.47	20.18
ZY1-23	2043.84	0.11	5.08	8.09	3.00	5.19	13.27
ZY1-24	2049.77	0.08	3.81	5.39	2.92	3.89	9.28

Funing Formation in the Subei Basin (Zhang et al., 2022b), suggesting greater light-oil loss in the current samples. A lower k_f further suggests that most of the light oil is lost. The relationship between total oil and S_1 is also significant, with total oil quantities substantially exceeding those of S_1. As a result, the corrections of light and heavy hydrocarbons are necessary for S_1. Fig. 2(b) exhibits the relationship between adsorbed oil ($S_{2\text{-}1}$) and S_2, indicating that more than half of S_2 originates from adsorbed oil. The adsorbed oil correction coefficient of S_2 (k_a) is about 0.54. Thus, the total oil of the AR shales can be estimated by adding $1.16S_1$ and $0.54S_2$.

The high contents of adsorbed oil result in an excellent correlation between total oil and adsorbed oil, as displayed in Fig. 2(c). Additionally, free oil also exhibits a robust correlation with total oil (Fig. 2(c)), implying that the resource sweet spot often refers to the free oil sweet spot (Li et al., 2018a; Zhang et al., 2022b). Organic matter serves as the primary adsorbent for shale oil (Wang et al., 2015). Thus, the strongest correlation is observed between TOC and adsorbed oil (Fig. 2(d)). There is also a significant relationship between total oil and TOC. In contrast, the weakest correlation is detected between free oil and TOC. This suggests that free oil is influenced by both organic matter content and pore structure in shale oil reservoirs (Bai et al., 2022; Zhang et al., 2023b; Wang et al., 2025c).

3.3. Shale oil occurrences determined by NMR

3.3.1. NMR T_2 spectra

NMR T_2 spectra of the selected shales at five states are presented in Fig. 3. The T_2 spectra are primarily trimodal, with the left peak located at T_2 less than about 3 ms, the middle peak within 3–20 ms, and the right peak larger than 20 ms, which is similar to the T_2 spectra in the Gulong and Gaoyou (Subei Basin) Sags (Zhang et al., 2024a, 2024b). The T_2 spectra at the AR state exhibit preponderant left peaks and minimal middle peaks, with right peaks nearly absent, suggesting a significant loss of movable oil (light oil), as corroborated by the low $S_{1\text{-}1}$ values listed in Table 2. Following water restoration, i.e., WR state, the left peaks show a substantial increase in amplitude and shift to higher T_2 values. On the contrary, the middle peaks change slightly, and the right peaks remain indistinct, indicating that the left peaks are primarily associated with pore water (Zhang et al., 2024a). The middle peaks show a clear increase, and the right peaks begin to appear in the WOR state, indicating that the middle and right peaks are predominantly associated with pore oil. Therefore, pore water mainly occurs in small pores less than 100 nm, while pores larger than 100 nm are primarily saturated with pore oil (Wang et al., 2024). After washing out the oil and drying, a notable left peak persists, which is primarily attributed to (quasi-)solid protons in kerogen, solid bitumen, and clay-bound water (primarily hydroxyl groups) (Li et al., 2018b). When the dry shales are saturated with oil, three peaks can be identified, characterized by a larger middle peak and a similar right peak, compared with the T_2 spectra at the WOR state. Thus, the pore oil occurring in large pores is hardly affected by pore water. Unfortunately, pore water and oil in various states cannot be well disclosed by the T_2 spectrum.

3.3.2. NMR T_1–T_2 spectra

NMR T_1–T_2 is an alternative and novel technique, and several T_1–T_2 patterns have been proposed for analyzing pore fluids in various states (Fleury and Romero-Sarmiento, 2016; Habina et al., 2017; Li et al., 2018b). As discussed, pore oil generally has a larger T_1/T_2 ratio than pore water, corresponding to pore oil located above water in shale oil reservoirs. Adsorbed fluids are mainly

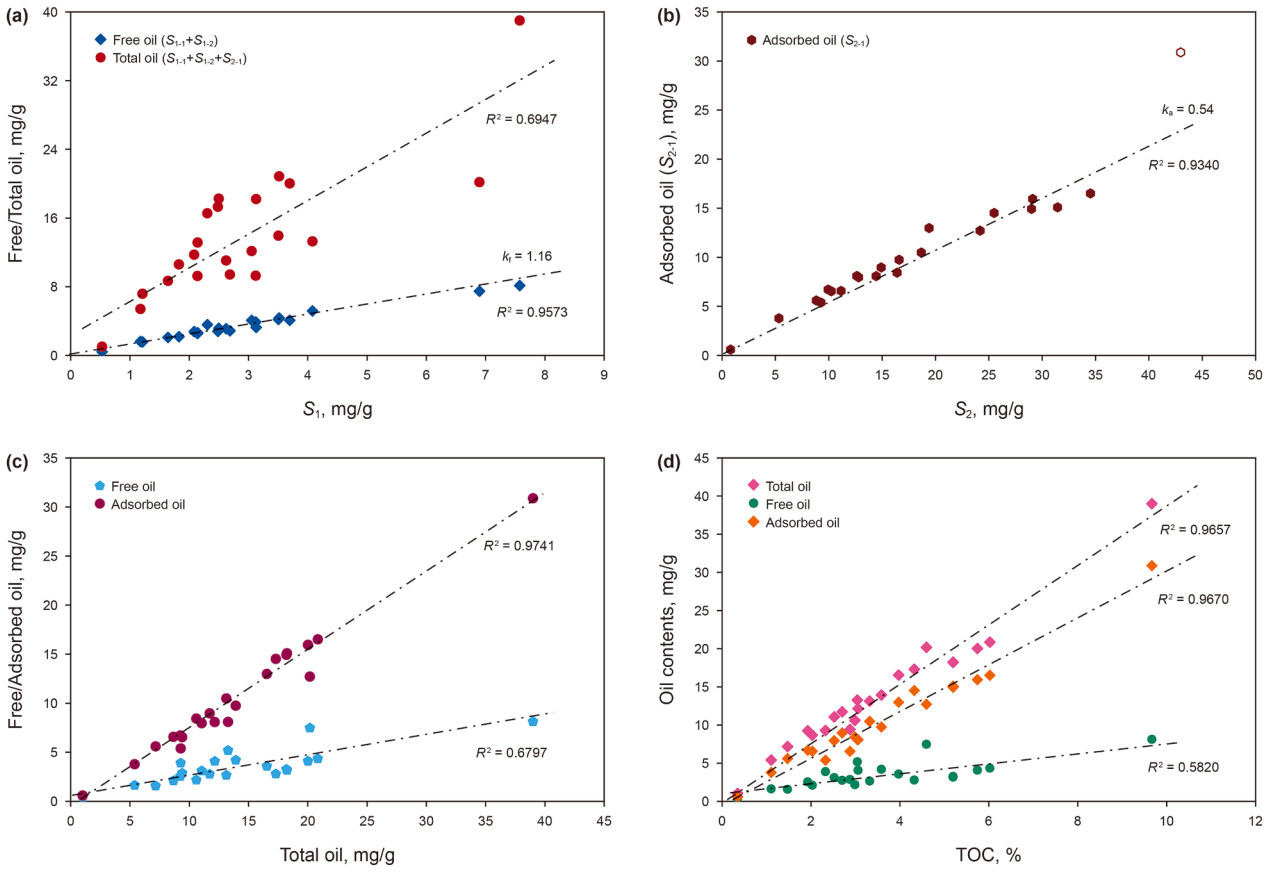

Fig. 2. Relationships among Rock-Eval parameters **(a–c)** and with TOC **(d)**.

characterized by higher T_1/T_2 ratios but lower T_2 values, and free fluids are the opposite (D'Agostino et al., 2014). Based on actual shale samples, a T_1–T_2 pattern using cluster analysis has been provided for shale oil reservoirs across eight regions, labeled A–H (Fig. 4) (Xiang et al., 2024; Zhang et al., 2024a, 2024b). T_1–T_2 spectra can well describe the dynamic changes in pore fluids in shale oil reservoirs across various states.

NMR T_1–T_2 spectra of the selected shales at five states are shown in Fig. 4. T_1–T_2 spectra at the AR state are notably characterized by a significant amplitude in Region A, with comparatively minor amplitudes observed in Regions B and C. However, Regions D and E are virtually indistinguishable, suggesting that nearly all movable fluids, including oil and water, have been depleted. Pore fluids of shales at the AR state primarily consist of capillary-bound water, adsorbed oil, and capillary-bound oil. After water restoration, the amplitude of Region A increases significantly, while Regions B and C exhibit minimal changes, further supporting the association of Region A with capillary-bound water. It also indicates that moisture re-enters the shale pore system after WR. As a result, pore fluids at WR are similar to the AR state, except for the restoration of pore water. However, Region E remains undetectable, which corresponds to the characteristic of shale reservoirs being typically defined by ultra-low water saturation levels, implying that water saturation is lower than that of capillary-bound water (Fang et al., 2014).

At the WOR state, the amplitude of Region C shows an outstanding increase, followed by Region D. As a result, capillary-bound and movable oil reappear in shale pore networks. Thus, compared with the AR state, nearly all movable oil and a portion of capillary-bound water and oil were lost during the pretreatment processes, such as coring and transportation. Fortunately, the lost oil and water can be reproduced after WOR. Thus, pore networks are saturated with pore fluids, and capillary-bound water, adsorbed oil, capillary-bound oil, and movable oil can be identified at the WOR state. After washing and drying, no amplitude is observed in Regions A to E, indicating the absence of pore fluid. When dry shale is saturated with oil, only oil is present in shale pores, and three regions can be identified: adsorbed, capillary-bound, and movable oil, with the T_2 value increasing in each. However, pore oil in the T_1–T_2 spectrum at the SO state shows a noticeable difference compared to that at the WOR state. Similar observations have been reported in previous studies (Zhang et al., 2022a, 2023b), suggesting that the presence of pore water significantly influences pore oil. Therefore, the in-situ occurrence characteristics of shale oil cannot be accurately represented by shales that have been saturated with oil.

3.3.3. *Comparisons of pore fluids in different states*

Quantitative analysis of amplitudes in Regions A to E is conducted to further investigate variations in pore fluids. The changes of pore fluids before and after WOR are discussed by comparing AR with WOR states, as displayed in Fig. 5. The capillary-bound water at the WOR state is much larger than that at AR state, with a slope greater than 1 and an intercept more than 0 (Fig. 5). The comparison between AR and WOR states from capillary-bound water indicates that almost half of the pore water has been lost, which is primarily controlled by the pore structures and relative humidity (Zhang et al., 2024a). A similar scene occurs for the total oil at the WOR and AR states (Fig. 5(b)), underscoring the importance of light hydrocarbon recovery for S_1. Surprisingly, adsorbed oil at the

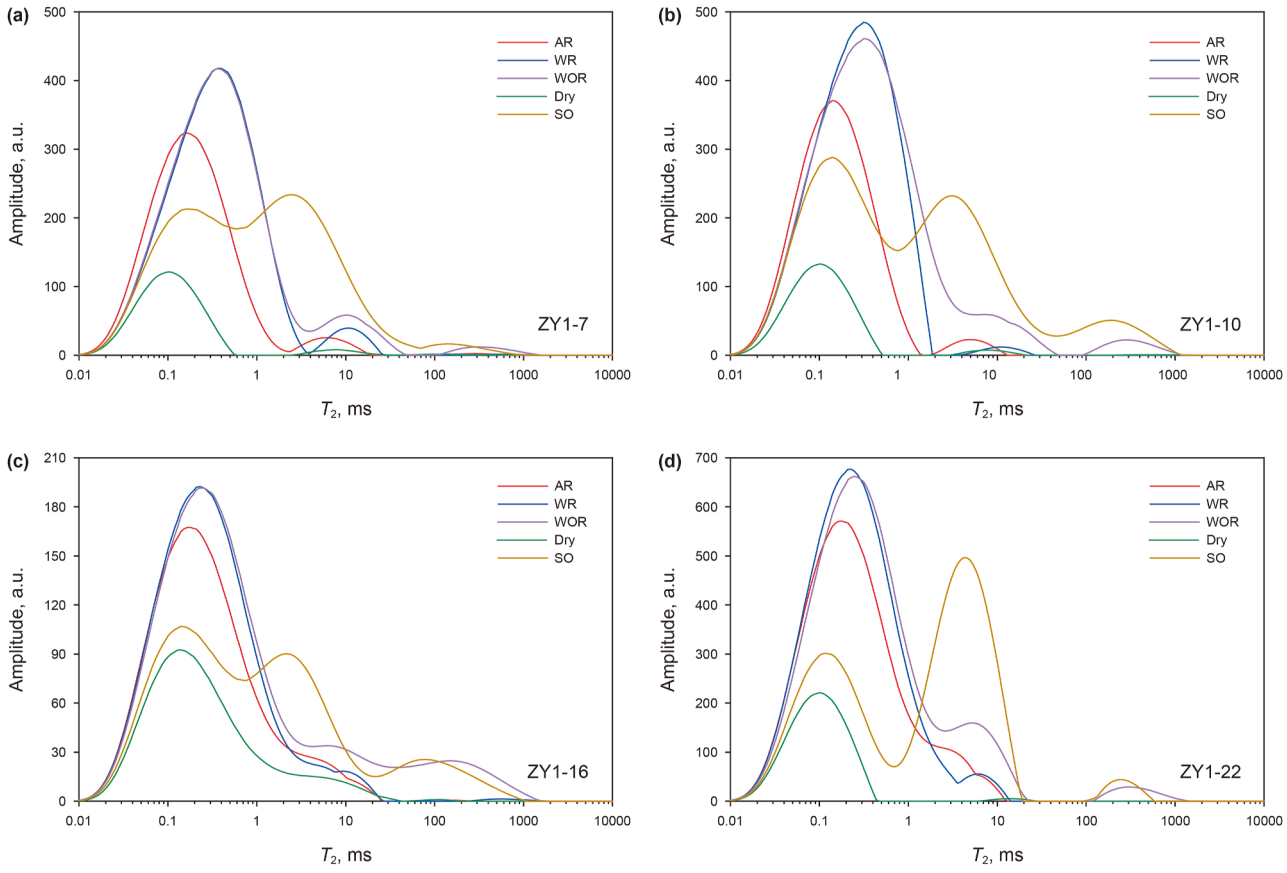

Fig. 3. NMR T_2 spectra comparison among different samples. AR, WR, WOR, Dry, and SO refer to the as-received, water restoration, water and oil restoration, oil-washed and dried, and oil-saturated states, respectively.

WOR state is generally larger than that at the AR state (Fig. 5(c)). This increase in adsorbed oil content can be attributed to the dissolution of solid bitumen and its subsequent adsorption onto pore surfaces during light oil saturation. Therefore, it can be inferred that the main cause of shale oil loss is the dispersion of light oil, leading to an increase in bitumen. A similar phenomenon, known as "component flow", has been discovered during the shale oil production process (Zhao et al., 2024). This phenomenon indicates that when shale oil is produced, light oil components are preferentially extracted.

Fig. 5(d) demonstrates that free oil at the WOR state is generally higher than that at the AR state, with an average loss of approximately 50% of the free oil. Shale samples typically exhibit greater capillary-bound oil contents at the WOR state compared to the AR state, as indicated in Fig. 5(e), corresponding to more than one-third of the capillary-bound oil loss. Meanwhile, movable oil contents before WOR are much lower than those at the WOR state (Fig. 5(f)), meaning that almost all the movable oil has been lost. As a result, the escapism of the shale pore fluids can be summarized as follows. After coring, due to the changes in temperature and pressure, pore oil and water in shale oil reservoirs gradually evaporate. The pore structures and ambient relative humidity primarily dictate the loss of pore water, with nearly half of the pore water being lost. Meanwhile, more than one-third of the capillary-bound oil is lost, and almost all movable oil vanishes. Furthermore, large-scale volatilization of light oil occurs, resulting in an increase in the solid bitumen content. Thus, the occurrence state of shale oil changes simultaneously during the loss process of pore fluids, which can be validated by the T_1–T_2 spectral distribution of the preserved shale core samples analyzed immediately and those exposed to open air at various time intervals (Li et al., 2022b).

T_1–T_2 spectra at WOR and SO states were compared to further disclose the influence of pore water on shale oil occurrence. A significant reduction in total oil content is observed in the WOR state relative to the SO state, as shown in Fig. 6(a). However, there is no obvious correlation of adsorbed oil between WOR and SO states (Fig. 6(b)), indicating that adsorbed oil is profoundly influenced by pore water, resulting in a decrease of adsorbed oil. Capillary-bound water at the SO state is more than that at the WOR state (Fig. 6(c)). Pore water occupies a substantial portion of the pore volume, consequently reducing the capillary-bound oil. Conversely, movable oil appears to be minimally influenced by pore water, as reflected in the strong correlation between the SO and WOR states for movable oil, as shown in Fig. 6(d).

3.3.4. *Pore fluid contents at AR and WOR states*

The amplitude in the NMR T_1–T_2 spectrum is directly proportional to the number of protons and should be equal to the amplitude in the T_2 spectrum if the test parameters are consistent (Zhang et al., 2019b; Xiang et al., 2024). Therefore, the calibration coefficients for pore water and oil can be determined from the amplitudes of T_2 spectra at different states (Xiang et al., 2024). This study obtained the calibration coefficient for pore water by comparing the T_2 spectra at the WR and AR states, yielding a value of 0.6581, with an extremely high correlation coefficient of 0.9778 (Fig. 7). The calibration coefficient for pore oil was determined by comparing the T_2 spectra at the SO and Dry states. A calibration coefficient of 0.5839 was obtained. These two calibration coefficients differ from those of the shales from the Gulong and

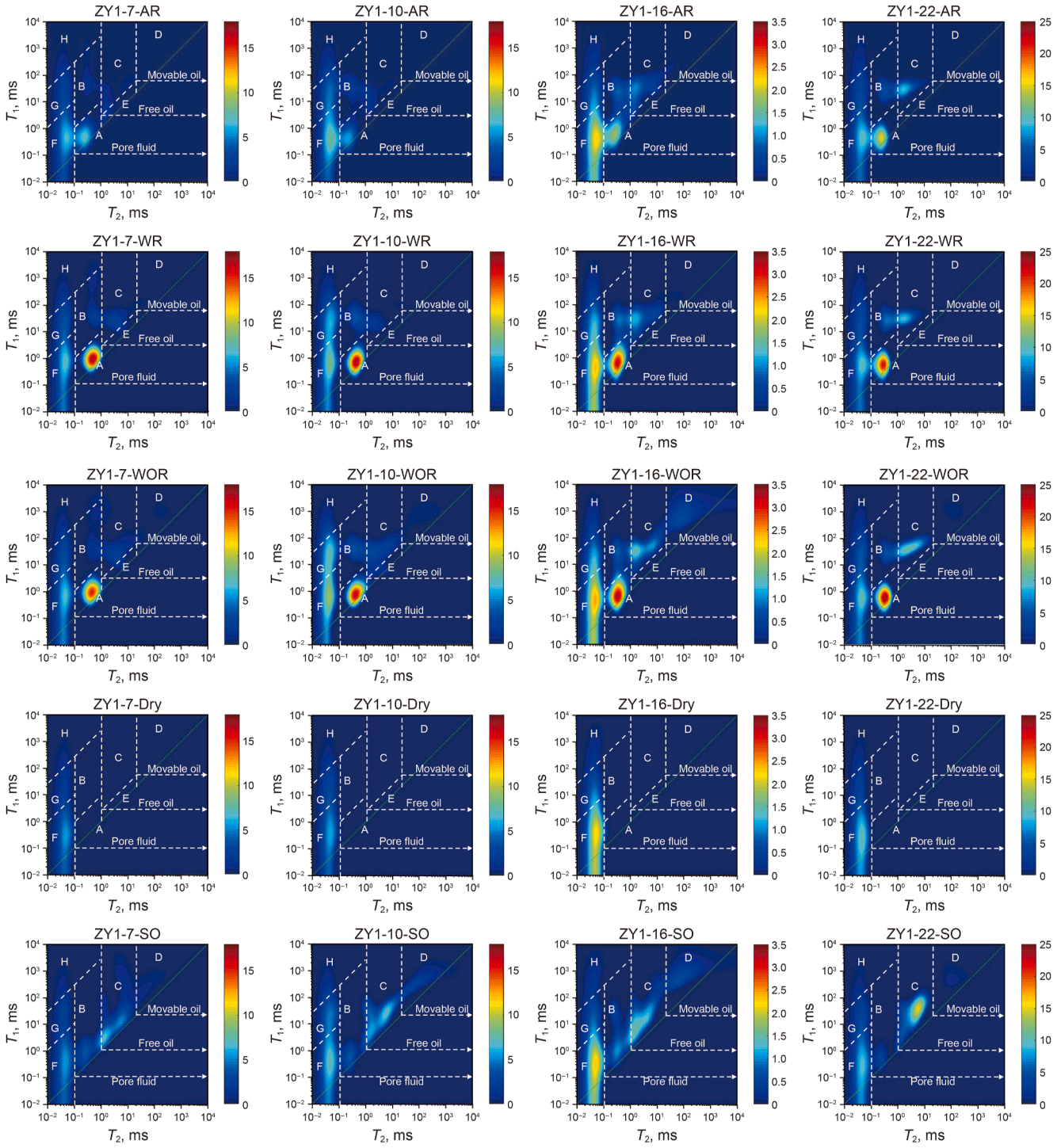

Fig. 4. NMR T_1–T_2 spectra at different states. A, B, C, D, and E refer to the capillary-bound water, adsorbed oil, capillary-bound oil, movable oil, and movable water; F, G, and H represent the clay-bound water, solid bitumen, and kerogen, respectively.

Gaoyou Sags, due to differences in maturity, mineral composition, etc. (Zhang et al., 2024a, 2024b).

According to the calibration coefficients, the contents of pore oil and water for AR shales in different states were quantitatively evaluated using T_1–T_2 spectra, as listed in Table 3. The capillary-bound water at the AR state has a larger average value of 21.76 mg/g, ranging from 1.23 mg/g to 48.61 mg/g, while the total oil is between 0.41 and 16.91 mg/g, with a mean of 5.70 mg/g. The shale oil at the AR state primarily consists of capillary-bound oil, with an average of 3.42 mg/g (0.11–9.70 mg/g), followed by adsorbed oil (mean 2.17 mg/g), while movable oil is characterized by a slight average of 0.14 mg/g (0.06–0.30 mg/g), corresponding to the lower $S_{1\text{-}1}$, with a mean of 0.13 mg/g (0.02–0.24 mg/g). Free oil varies from 0.27 mg/g to 10.00 mg/g, with a mean of 3.53 mg/g. The pore water and oil contents in the primary five lithologies vary significantly. CR shales have the lowest capillary-bound water (mean 5.39 g/g), followed by FR shales (mean 12.15 mg/g), due to the lowest clay mineral contents. On the contrary, FAM shales,

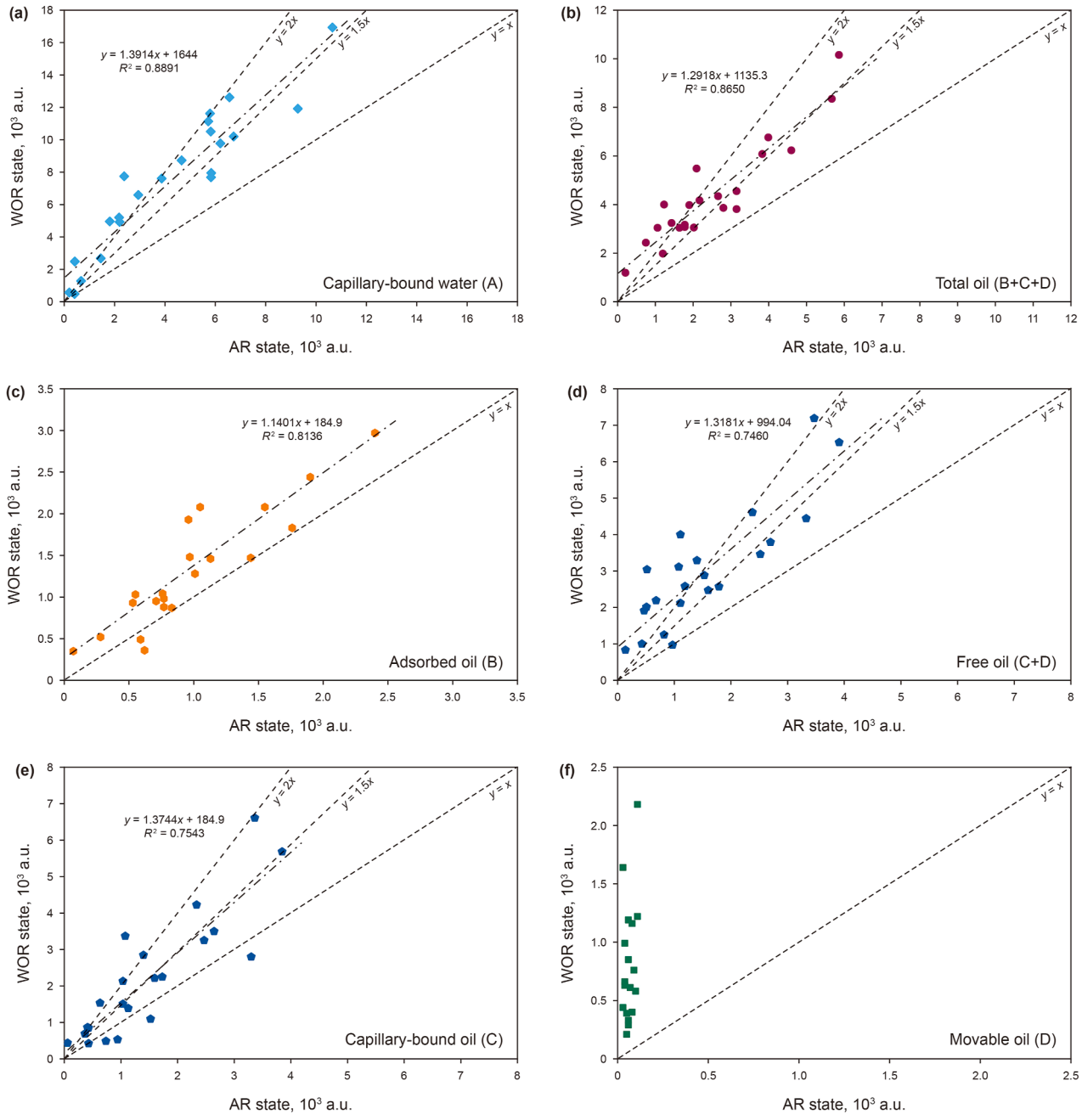

Fig. 5. Relationships of capillary-bound water **(a)**, total oil **(b)**, adsorbed oil **(c)**, free oil **(d)**, capillary-bound oil **(e)**, and movable oil **(f)** between AR and WOR states.

with the largest clay mineral contents, are characterized by the largest contents of capillary-bound water (mean 40.38 mg/g). A conclusion can be drawn that a higher clay mineral content is generally associated with a greater amount of capillary-bound water (Xiang et al., 2024). High total and free oil contents generally occur in CR and FAM shales, while low total oil and extensive adsorbed oil contents are mainly discovered in CBAFR shales.

Pore water and oil contents of the selected shales at the WOR state are shown in Table 4. The average of capillary-bound water increases to 39.49 mg/g, with a range of 3.50–73.30 mg/g, much larger than that at the AR state (mean 21.76 mg/g). Movable oil increases significantly, with an average of 1.63 mg/g (0.54–4.34 mg/g), while the capillary-bound oil averages 5.18 mg/g, between 0.84 and 19.04 mg/g. A slight increase is also observed for adsorbed oil, with a mean of 2.97 mg/g (0.65–8.57 mg/g). As a result, free oil is characterized by a large average content of 6.81 mg/g, ranging from 1.60 mg/g to 20.71 mg/g. Correspondingly, the oil saturation (S_o) can be acquired, varying from 7.74% to 85.06%, with a low mean of 30.18%, which is much lower than that of shales with low clay mineral contents (Xiang et al., 2024). Thus, a higher content of clay minerals primarily relates to a larger content of pore water (mainly capillary-bound water), corresponding to a lower oil saturation in shale oil reservoirs.

After water and oil restoration, the capillary-bound water in CR shales is the lowest, with an average of 10.95 mg/g, followed by the FCM shales (mean 25.41 mg/g), corresponding to a larger oil saturation in CR and FCM shales. FAM shales have the largest capillary-bound water (mean 63.49 mg/g), and CBAFR shales are

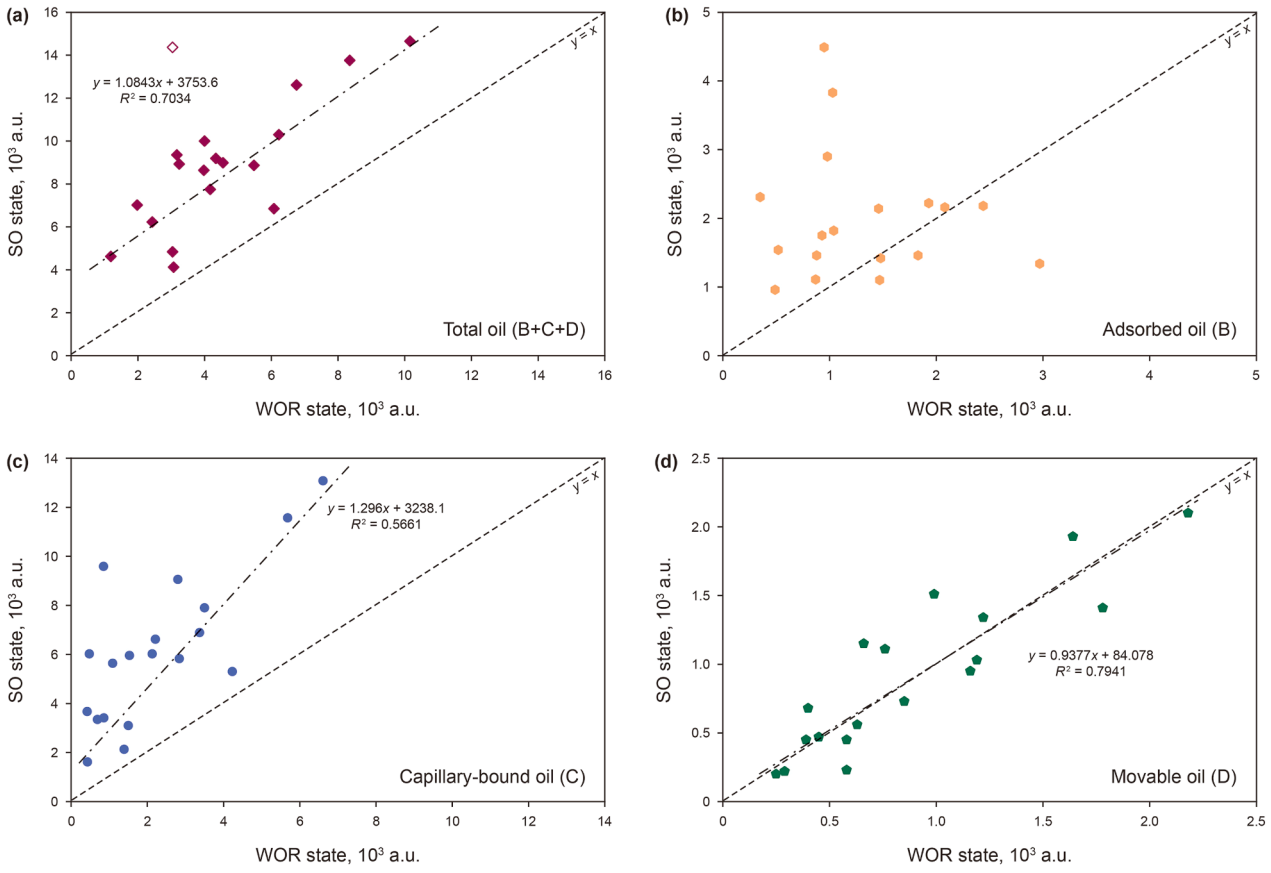

Fig. 6. Relationships of total oil **(a)**, adsorbed oil **(b)**, capillary-bound oil **(c)**, and movable oil **(d)** between SO and WOR states.

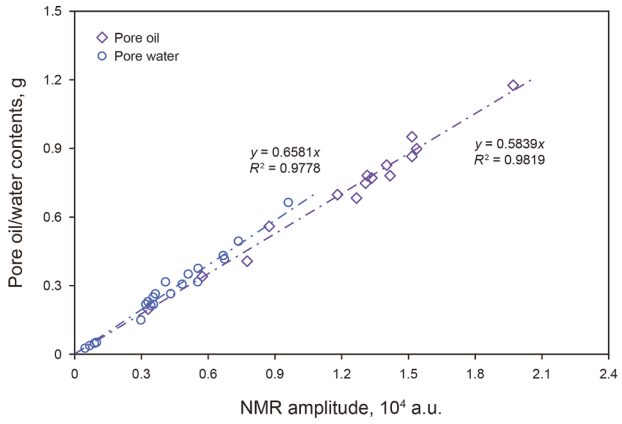

Fig. 7. Pore oil and water calibrations of NMR amplitudes.

the second (49.77 mg/g), with lower oil saturations of 20.09% and 20.04%, respectively. Significant increases are identified in capillary-bound water and free oil for FR shales, implying more large pores and better pore structures in FR shales. And FR shales have the highest average free oil content (mean 9.62 mg/g). Thus, the FR shale may be the optimal lithology for shale oil in the Qingshankou Formation of the Sanzhao Sag. The relationships between total oil and shale oil in adsorbed, capillary-bound, and movable states indicate that shale oil primarily consists of capillary-bound oil, followed by adsorbed oil, with a low content of movable oil (Fig. 8).

Table 3
Pore oil and water contents at the AR state obtained from NMR T_1–T_2 spectra.

Samples	Lithologies	A, mg/g	B, mg/g	C, mg/g	D, mg/g	Total oil, mg/g	Free oil, mg/g
ZY1-1	CR	11.04	0.13	0.11	0.16	0.41	0.27
ZY1-2	CBAFR	38.09	1.72	0.96	/	2.68	0.96
ZY1-3	CBAFR	32.76	0.65	0.51	0.10	1.25	0.60
ZY1-5	CBAFR	31.87	2.02	1.55	0.18	3.75	1.73
ZY1-6	CBAFR	31.91	2.24	2.02	0.07	4.33	2.08
ZY1-7	FR	21.00	1.10	2.16	0.16	3.41	2.31
ZY1-8	FR	10.13	0.60	0.78	0.23	1.62	1.02
ZY1-9	CBCFR	32.13	1.41	0.82	0.22	2.44	1.04
ZY1-10	FR	14.30	2.25	2.49	0.08	4.82	2.57
ZY1-11	CR	1.23	3.37	5.47	0.11	8.95	5.58
ZY1-12	FCM	12.06	4.03	5.62	0.12	9.78	5.75
ZY1-13	CBAFR	25.93	3.32	3.42	/	6.74	3.42
ZY1-14	FCM	30.88	1.54	1.29	0.09	2.92	1.38
ZY1-16	CBAFR	5.03	0.79	1.51	0.08	2.38	1.59
ZY1-17	CBAFR	31.19	1.70	2.12	0.08	3.91	2.21
ZY1-18	FCM	3.51	2.06	3.51	0.11	5.68	3.62
ZY1-19	CBAFR	20.53	2.07	3.75	/	5.82	3.75
ZY1-20	FR	3.15	6.91	9.70	0.30	16.91	10.00
ZY1-21	CR	3.91	2.32	9.16	0.19	11.67	9.35
ZY1-22	CBAFR	37.28	3.76	8.18	0.13	12.07	8.31
ZY1-23	FAM	32.15	1.41	7.05	0.06	8.52	7.11
ZY1-24	FAM	48.61	2.28	3.07	/	5.35	3.07

A, B, C, and D refer to capillary-bound water, adsorbed oil, capillary-bound oil, and movable oil, respectively.

3.3.5. Comparison between Rock-Eval and NMR T_1–T_2

Rock-Eval, especially multi-stage Rock-Eval, and NMR T_1–T_2 are regarded as key techniques in detecting shale oil contents (Zhang et al., 2022b; Li et al., 2022a, 2022b). A series of comparisons

Table 4
Pore oil and water contents at the WOR state obtained from NMR T_1–T_2 spectra.

Samples	Lithologies	A, mg/g	B, mg/g	C, mg/g	D, mg/g	S_{tr}, mg/g	S_{fr}, mg/g	S_{fr}/S_1	S_o, %
ZY1-1	CR	24.70	0.68	0.84	0.77	2.29	1.60	3.03	11.46
ZY1-2	CBAFR	73.30	2.20	0.94	1.29	4.42	2.23	1.04	7.74
ZY1-3	CBAFR	52.09	1.22	1.00	1.38	3.60	2.38	1.45	8.80
ZY1-5	CBAFR	57.54	4.05	1.02	1.61	6.68	2.63	0.84	13.93
ZY1-6	CBAFR	62.13	4.46	1.14	0.94	6.53	2.08	1.00	12.82
ZY1-7	FR	41.27	1.93	3.13	1.28	6.34	4.41	2.06	17.68
ZY1-8	FR	27.72	1.12	1.47	2.62	5.22	4.10	3.48	20.85
ZY1-9	CBCFR	50.66	1.90	1.72	4.34	7.96	6.06	5.00	18.01
ZY1-10	FR	46.59	3.43	7.78	1.46	12.67	9.24	3.72	27.55
ZY1-11	CR	3.50	3.44	9.89	0.90	14.24	10.79	4.68	85.06
ZY1-12	FCM	28.77	5.19	7.43	0.62	13.24	8.05	2.29	39.15
ZY1-13	CBAFR	48.62	4.46	4.74	0.54	9.74	5.28	1.43	21.87
ZY1-14	FCM	40.68	2.12	3.12	1.34	6.59	4.47	1.70	18.47
ZY1-16	CBAFR	9.33	0.65	1.85	1.59	4.10	3.45	1.13	38.07
ZY1-17	CBAFR	42.47	1.78	4.37	2.03	8.18	6.39	3.50	21.21
ZY1-18	FCM	6.77	2.60	4.56	0.66	7.82	5.22	2.09	61.76
ZY1-19	CBAFR	45.96	2.35	7.62	1.20	11.17	8.82	2.52	25.37
ZY1-20	FR	18.62	8.57	19.04	1.67	29.28	20.71	2.73	68.74
ZY1-21	CR	4.64	1.32	12.06	0.77	14.15	12.83	4.77	74.67
ZY1-22	CBAFR	56.50	3.89	12.09	1.80	17.78	13.89	2.01	30.56
ZY1-23	FAM	64.57	4.96	5.97	3.50	14.44	9.48	2.32	23.82
ZY1-24	FAM	62.41	2.94	2.20	3.59	8.73	5.79	1.85	16.36

A, B, C, and D refer to capillary-bound water, adsorbed oil, capillary-bound oil, and movable oil, respectively; S_{tr} and S_{fr} represent the total and free oil saturations at WOR state, respectively; S_o: oil saturation.

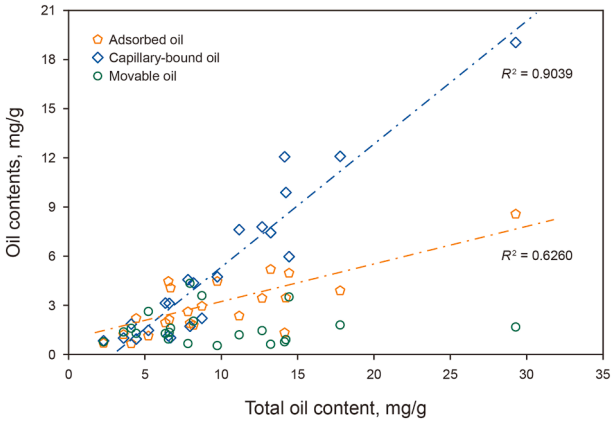

Fig. 8. Correlations of total oil with adsorbed, capillary-bound, and movable oil at the WOR state.

between Rock-Eval and NMR T_1–T_2 are performed and exhibited in Fig. 9. Total oil at the AR state from the T_1–T_2 spectrum correlates well with the total oil determined by multi-stage Rock-Eval, as shown in Fig. 9(a). However, NMR T_1–T_2 spectral total oil falls short of that reported by the multi-stage Rock-Eval. On the contrary, S_1 is generally lower than the total oil derived from T_1–T_2 spectra, implying that heavier hydrocarbons must be considered when estimating total oil content based on S_1 (Zhang et al., 2022b). Fig. 9(b) shows that the free oil detected by NMR correlates well with the free oil and S_1 values obtained from Rock-Eval. The sample crushing process results in the loss of more hydrocarbons, which accounts for the lower free oil measurements by Rock-Eval in shales with substantial free oil content. A similar scene was also observed in shales from the Funing Formation in the Gaoyou Sag (Zhang et al., 2024a).

Furthermore, free oil measured by NMR is commonly much larger than that determined by Rock-Eval for the preserved or fresh shales (Li et al., 2022b; Zhang et al., 2024b). Nevertheless, the adsorbed oil obtained from the T_1–T_2 spectra is much lower than that obtained from the Rock-Eval (Fig. 9(c)). T_1–T_2 spectral adsorbed oil is primarily linked to oil adsorbed on the pore surfaces, while the $S_{2\text{-}1}$ consists of oil adsorbed on the pore surfaces and oil absorbed in organic matter (Zhang et al., 2024b). The latter mainly occurs in Regions G or H in the T_1–T_2 spectrum. The NMR T_1–T_2 spectrum primarily characterizes pore oil and contributes to the precise evaluation of free oil.

Rock-Eval parameter S_1 is the most widely used parameter for evaluating shale oil content (Wang et al., 2022a; Xu et al., 2022). Due to changes in pressure and temperature, the tested S_1 of the AR shales usually lacks a significant portion of light hydrocarbons (C_{14-}), with higher maturity levels leading to greater losses of these light hydrocarbons (Ma et al., 2024; Sun et al., 2024a). Previous studies have provided multiple methods for the correction of light hydrocarbons for S_1, such as hydrocarbon-generating kinetics (Xue et al., 2016), preserved shales (Ma et al., 2024; Sun et al., 2024a), liquid-nitrogen freezing shales (Zhang et al., 2022b), etc. In this study, an innovative approach is introduced to compensate for the loss of light hydrocarbons in S_1. The free oil, a sum of capillary-bound and movable oil, at the WOR state effectively reflects the in-situ free oil in shales and shows a good correlation with S_1 (Fig. 9(d)). The recovery coefficient of free oil for S_1 is about 2.3, which agrees well with the free oil recovery coefficients determined by the preserved shales reported in previous studies (Ma et al., 2024; Sun et al., 2024a). Moreover, there is a good relationship between S_1 and the total oil at the WOR state. Thus, the recovery method for oil and water employed in this study can effectively replicate the in-situ pore fluids of shale oil reservoirs, offering an innovative and practical approach to correct light hydrocarbons in S_1.

3.4. Pore structures

The micro-occurrence of pore fluids is directly constrained by pore types and associated minerals in shale reservoirs (Gao et al., 2022; Xue et al., 2022). Clay minerals are hydrophilic, leading to the pores associated with clay minerals being primarily saturated with water (Zolfaghari et al., 2017a, 2017b). On the contrary, organic pores are lipophilic and are primarily filled with hydrocarbons or methane (Cheng et al., 2019). Pore types and distributions are well displayed by high-resolution SEM images, as shown in Fig. 10. The CBAFR shales are rich in clay minerals and quartz, leading to the formation of intraparticle pores within clay mineral aggregates and interparticle pores at the edges of quartz grains (Fig. 10(a)). Meanwhile, fractures are also observed. With clay minerals decreasing, the interparticle pores between or at the edge of quartz or feldspar are the most common in the FR shales (Fig. 10(b)). The developed interparticle pores between calcite granules are the main features of the CR shales (Fig. 10(c)). As shown in Fig. 10(d), plenty of interparticle pores occur in the FCM shales. On the contrary, a significant number of intraparticle pores are identified in the FCM shales, attributable to their high clay mineral content.

Pore fluids and their occurrence states are primarily controlled by the pore structures of shales (Li et al., 2017). Adsorbed fluids are mainly associated with pore surfaces, which can be well measured by LTNA/D (Li et al., 2018a). The NMR T_2 spectrum reflects the full-scale PSD in shales and can be quantitatively calibrated by LTNA/D and SEM (Zhang et al., 2019b). The BET SSA and full-scale PSDs can be determined and listed in Table 5. The BET SSA of the studied shales varies significantly, ranging from 1.32 m^2/g to 31.23 m^2/g, with a mean of 14.26 m^2/g. The shale samples mainly consist of mesopores, with an average porosity of 3.24% (0.85%–6.98%), followed by micropores (mean 2.85%), minipores (mean 1.95%), and

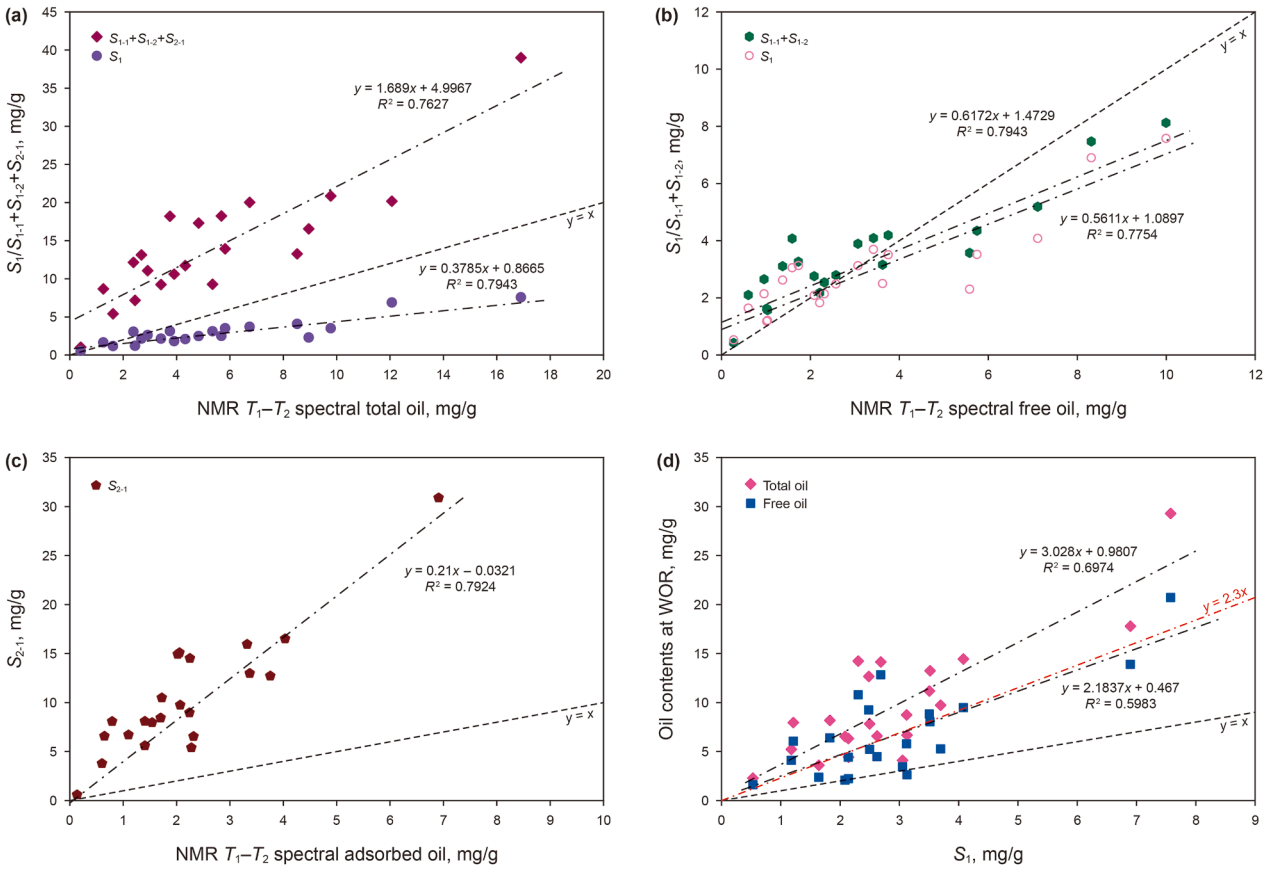

Fig. 9. Relationships of total oil **(a)**, free oil **(b)**, and adsorbed oil **(c)** between Rock-Eval and NMR at the AR state and the correlations of S_1 with total and free oil at the WOR state **(d)**.

macropores (mean 1.02%). Correspondingly, mesopores have the largest percentage, averaging 34.59%, while micropores have a larger average of 33.61%. The CR shales have the lowest BET SSA (mean 7.10 m^2/g), which is beneficial for the occurrence of free oil. A lower average BET SSA (mean 9.69 m^2/g) value of the FR shales is observed, which is related to the largest porosity of mesopores (mean 3.63%) and macropores (mean 1.57%). Conversely, the CBAFR shales have larger BET SSA values (mean 23.51 m^2/g), but lower porosity of mesopores (mean 2.84%) and macropores (mean 0.82%). As a result, FR shales may be favorable shale oil reservoirs, with the development of interparticle pores, lower BET SSA, and abundant meso- and macropores, which are beneficial for the enrichment of free oil.

3.5. Controlling factors of shale oil occurrence

3.5.1. Organic matter and mineral compositions

Organic matter plays a pivotal role in the enrichment of shale oil and serves as the primary adsorbent for adsorbed oil (Wang et al., 2015; Zhang et al., 2022b). A larger TOC value is generally indicative of a greater shale oil content, and an increased organic matter content correlates with higher adsorbed oil content and a lower proportion of free oil (Zhang et al., 2022b). The relationships between TOC and shale oil contents in different states at the WOR state are displayed in Fig. 11(a). There is a good correlation between TOC and adsorbed oil, with the largest correlation coefficient; however, this is significantly lower than the correlation between TOC and S_{2-1} (Fig. 2(d)). This further suggests that adsorbed oil tested by NMR primarily refers to the oil adsorbed on the pore surfaces, excluding the oil absorbed within the organic matter. A weak positive correlation is identified between TOC and capillary-bound oil, while movable oil shows no obvious relationship with TOC. Thus, the free oil, i.e., capillary-bound and movable oil, is also restricted by the pore structures, especially movable oil (Li et al., 2018a; Zhang et al., 2023b). Accordingly, a weak correlation is observed between total oil content and TOC. Pore water is predominantly found in pores associated with hydrophilic clay minerals (Zolfaghari et al., 2017a, 2017b), leading to a strong correlation between capillary-bound water and clay minerals, as shown in Fig. 11(b). Therefore, a high content of clay minerals is detrimental to the enrichment of shale oil.

3.5.2. Pore structure parameters

As discussed, pore fluids are also constrained by the pore structures of shales. Minerals in shale oil reservoirs tend to be more hydrophilic, making water more likely to be adsorbed onto pore surfaces (Bai et al., 2020). As exhibited in Fig. 12, capillary-bound water correlates well with BET SSA, while there is no relationship between adsorbed oil and BET SSA. Thus, pore water will severely affect adsorbed oil, resulting in a much lower adsorbed oil content than in the SO state. Capillary-bound water is primarily related to intraparticle pores in clay mineral aggregates at small scales. Thus, capillary-bound water mainly occurs in micro- and minipores, characterized by a positive correlation between the two (Fig. 13(a)). Previous studies have indicated that adsorbed oil primarily occurs in small pores, while large pores are mainly saturated with free oil (Li et al., 2018b; Zhang et al., 2022a, 2023b). However, an unexpected phenomenon occurs: there is no

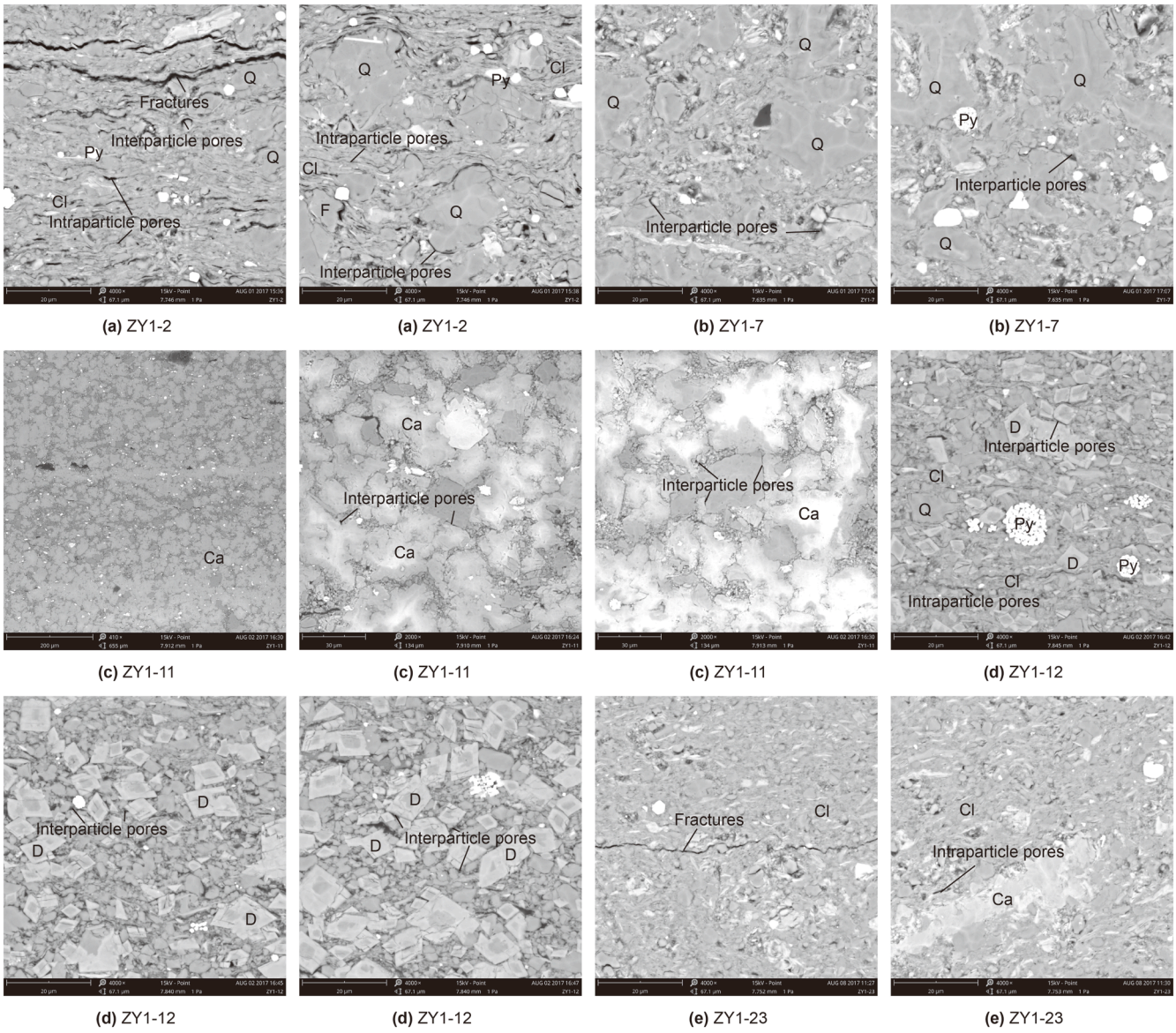

Fig. 10. SEM images of the studied shales in different lithologies. **(a)** ZY1-2, 1931.20 m, K_1qn^{2+3}, CBAFR shale, intraparticle pores in clay mineral aggregates, interparticle pores at the edge of quartz, and fractures; **(b)** ZY1-7, 1958.1 m, K_1qn^{2+3}, FR shale, interparticle pores between or at the edge of quartz or feldspar; **(c)** ZY1-11, 1980.95 m, K_1qn^1, CR shale, interparticle pore between calcite granules; **(d)** ZY1-12, 1993.30 m, K_1qn^1, FCM shale, interparticle pores; **(e)** ZY1-23, 2043.84 m, K_1qn^1, FAM shale, intraparticle pores in clay mineral aggregates and fractures. Q: quartz; O: orthoclase; F: feldspar; Ca: Calcite; D: dolomite; Cl: clay minerals; Py: pyrite.

Table 5
Pore structure parameters of the selected shales.

Sample	Lithologies	BET SSA, m^2/g	Porosity of various scale pores, %				Pore percentage content, %			
			Micro-	Mini-	Meso-	Macro-	Micro-	Mini-	Meso-	Macro-
ZY1-1	CR	12.87	1.82	1.18	0.85	0.37	43.09	28.00	20.04	8.87
ZY1-2	CBAFR	31.23	4.31	2.06	2.02	1.27	44.66	21.28	20.96	13.10
ZY1-5	CBAFR	25.34	4.09	2.26	2.70	0.85	41.32	22.82	27.27	8.59
ZY1-7	FR	14.95	2.73	2.34	2.81	0.67	31.94	27.33	32.86	7.86
ZY1-8	FR	8.94	2.81	1.43	1.17	0.85	44.82	22.90	18.75	13.53
ZY1-10	FR	12.47	3.72	2.20	3.55	1.42	34.13	20.22	32.60	13.04
ZY1-11	CR	1.32	1.33	1.45	3.32	0.27	20.92	22.81	52.08	4.19
ZY1-12	FCM	12.05	2.67	2.03	3.93	0.64	28.83	21.91	42.40	6.86
ZY1-13	CBAFR	18.74	3.25	2.36	3.00	0.75	34.75	25.21	32.08	7.96
ZY1-19	CBAFR	18.72	1.96	1.97	3.66	0.40	24.50	24.63	45.82	5.05
ZY1-20	FR	2.41	2.85	2.01	6.98	3.32	18.76	13.25	46.06	21.93
ZY1-23	FAM	12.03	2.63	2.11	4.91	1.48	23.59	18.99	44.15	13.27

Micro-, mini-, meso-, and macro-denote the micropores, minipores, mesopores, and macropores, respectively.

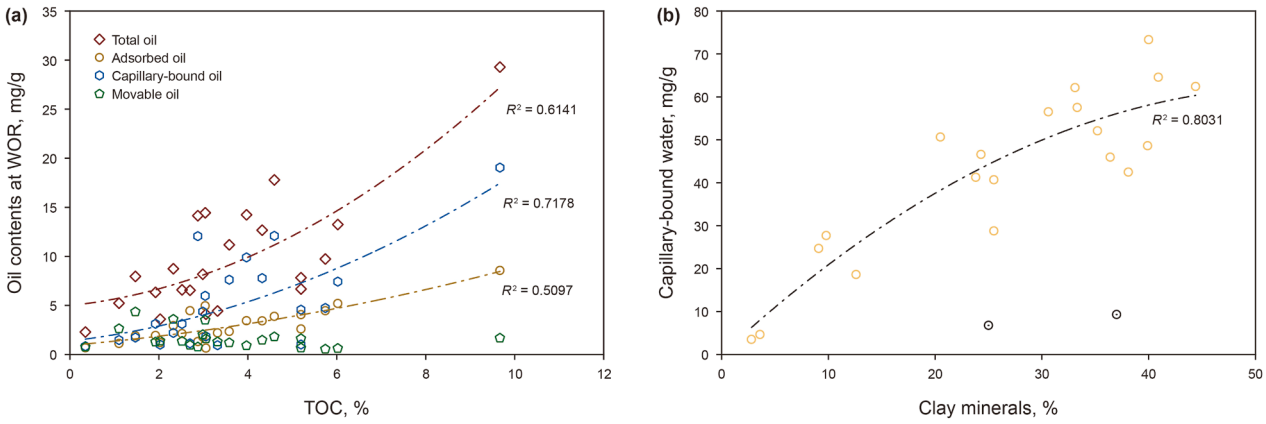

Fig. 11. **(a)** Correlations between TOC and shale oil contents at WOR state; **(b)** relationship between clay minerals and capillary-bound water.

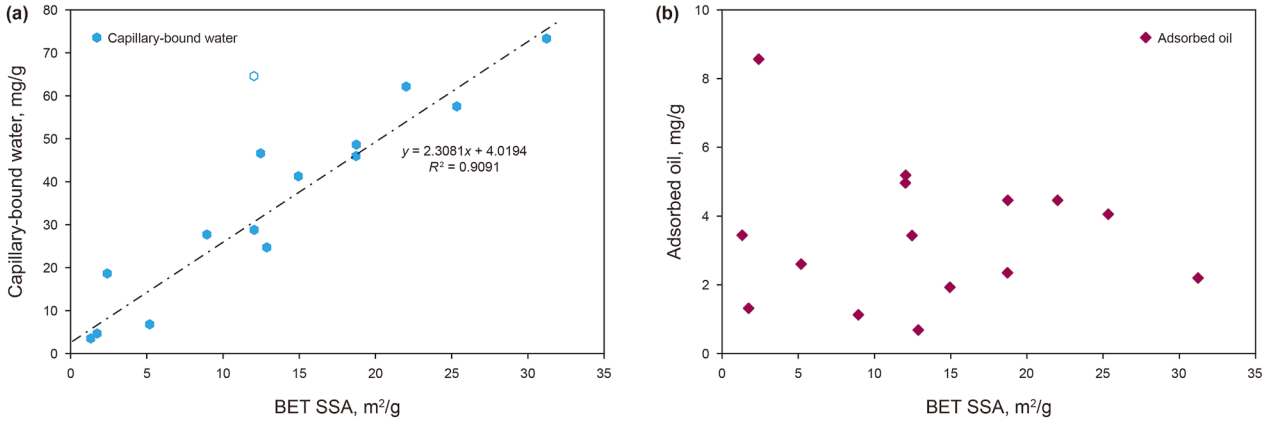

Fig. 12. Relationships between BET SSA with capillary-bound water **(a)** and adsorbed oil **(b)**.

relationship between adsorbed oil and pores less than 100 nm (micro- and minipores), as shown in Fig. 13(b). A possible explanation for this is that micro- and minipores are primarily saturated with capillary-bound water, leaving few surfaces available for oil adsorption.

On the contrary, a series of excellent positive correlations are observed between mesopores and total, capillary-bound, and adsorbed oil, suggesting that shale oil primarily resides in mesopores, with capillary-bound oil in particular showing the largest correlation coefficient (Fig. 13(c)). This finding, however, presents a discrepancy with previous studies on adsorbed oil (Li et al., 2018b; Zhang et al., 2022a, 2023b). The selected shales exhibit a strong relationship between adsorbed oil and mesopores, which may be attributed to autocorrelation. The total oil content shows significant correlations with both mesopores and adsorbed oil (Fig. 8), leading to a strong association between mesopores and adsorbed oil. Movable oil does not exhibit a relationship with mesopores but instead shows a positive correlation with macropores. This implies that movable oil is primarily located in macropores, as evidenced by the appearance of right peaks in T_2 spectra after WOR (Fig. 3).

3.6. Occurrence pattern of shale pore fluids

The effective development of shale oil is primarily controlled by the contents and occurrences of pore fluids in different states. Previous studies have reported pore-fluid occurrence patterns in oil-saturated shales (Zhang et al., 2022a, 2023b). Specifically, adsorbed oil is predominantly found in micro- and minipores, capillary-bound oil is commonly present in mesopores, and macropores are primarily filled with movable oil. Unfortunately, these patterns ignore pore water. As discussed, the NMR T_1–T_2 spectrum offers an alternative technique to visually display the micro-scale distribution of shale pore fluids, effectively revealing capillary-bound water, adsorbed oil, capillary-bound oil, and movable oil. Accurately determining the occurrence PSDs of these pore fluids remains challenging (Wang et al., 2024). NMR T_1–T_2 spectra have been less effective in characterizing the PSDs of shales, whereas the T_2 spectrum excels in exploring pore sizes (Zhang et al., 2019b). Wang et al. (2024) developed a T_2 spectral peaking treatment method based on the Gaussian Function. As a result, T_2 spectra of capillary-bound water, adsorbed oil, capillary-bound oil, and movable oil can be extracted according to the T_2 spectrum at the WOR state. Then, the occurrence PSDs can be determined. This study adopted this method to obtain the micro-occurrence distributions of pore fluids in shale oil reservoirs. The pattern of pore fluid occurrence in shale oil reservoirs is established and exhibited in Fig. 14.

Capillary-bound water is primarily located at T_2 values less than 10 ms, corresponding to pores smaller than 100 nm, i.e., micro- and minipores. The T_2 values for adsorbed oil range from 0.05 ms to 4 ms and overlap with that of capillary-bound water. Adsorbed oil mainly occurs in micro- and minipores, and so does capillary-bound water. As a result, pore water significantly reduces adsorbed oil, leading to a significant decrease in adsorbed oil (Fig. 6(b)). Capillary-bound oil exhibits T_2 values between 2 ms and

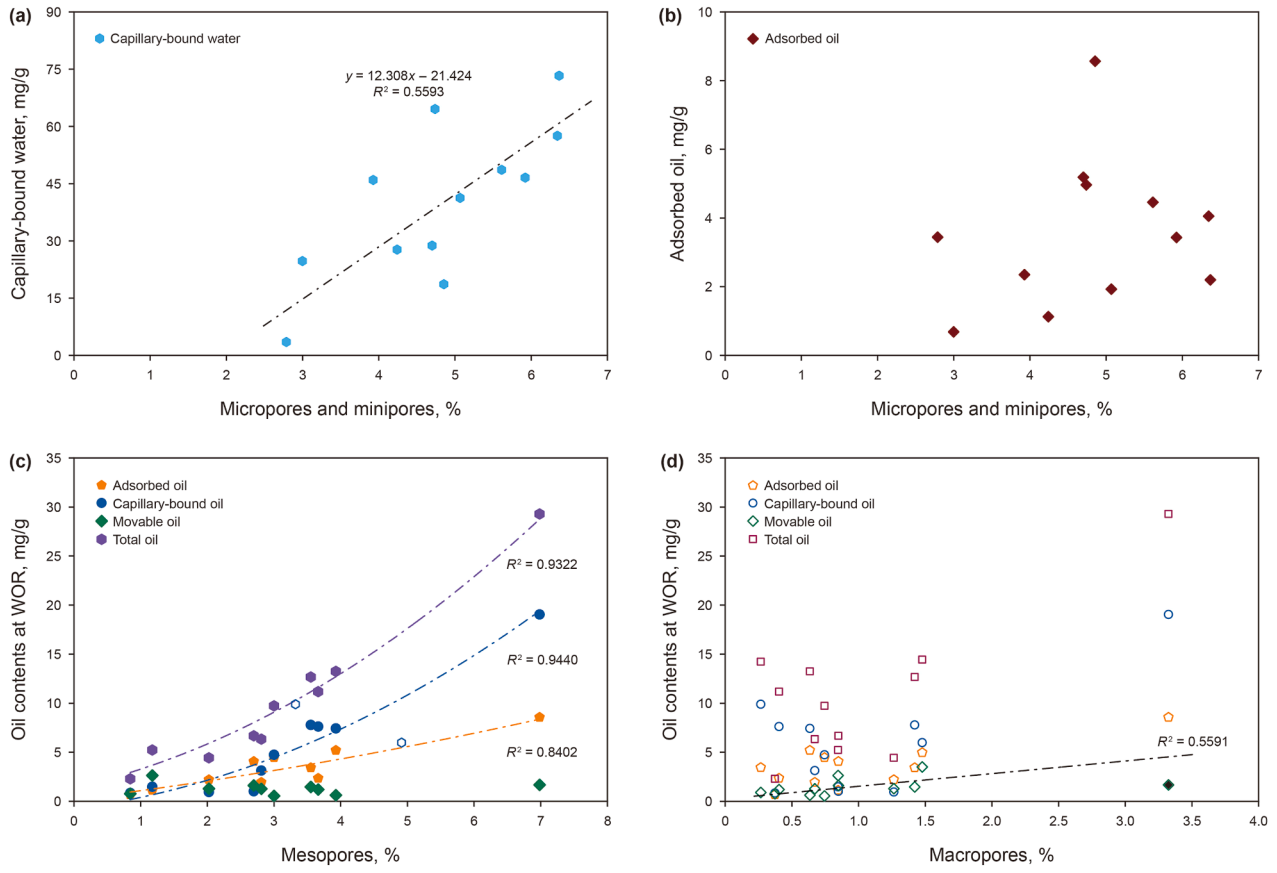

Fig. 13. Correlations of micro- and minipores with capillary-bound water **(a)** and adsorbed oil **(b)**, relationships between mesopores and shale oil contents **(c)**, and relationships of macropores and shale oil contents **(d)**.

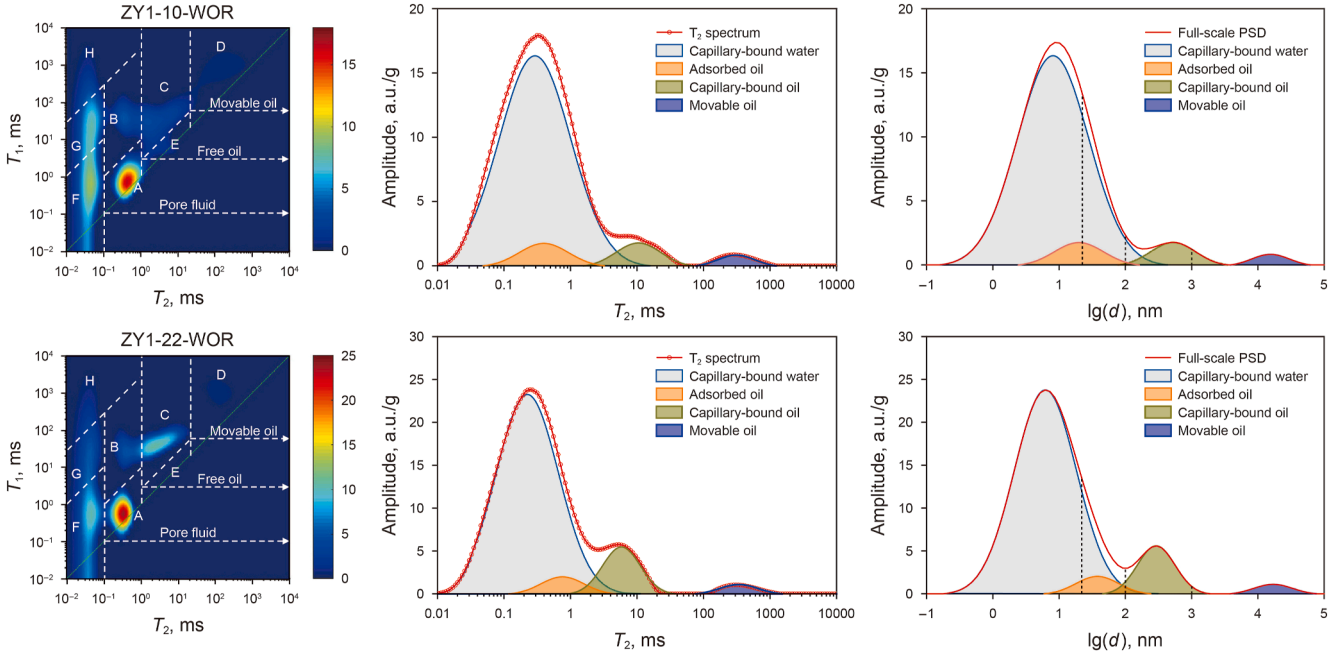

Fig. 14. Pore fluid occurrence pattern in shale oil reservoirs.

50 ms and primarily resides in mesopores. Movable oil has the largest T_2 values, ranging from 100 ms to 2000 ms, meaning that macropores are mainly saturated with movable oil. Thus, it can be inferred that in shale oil reservoirs, micropores and mini-pores are generally saturated with capillary-bound water and a minor fraction of adsorbed oil. In contrast, mesopores and macropores are

chiefly responsible for the accumulation of capillary-bound and movable oil, respectively. Enhancing mesopore and macropore development is advantageous for enriching shale oil, particularly free oil, as observed in the FR shale in this study (Sun et al., 2024b). As a result, the FR shale is regarded as an ideal lithology for shale oil enrichment in the Sanzhao Sag, with plenty of interparticle pores, low content of clay minerals (mean 17.63%), low BET SSA (mean 9.69 m^2/g), high porosity of mesopores (mean 3.63%) and macropores (mean 1.57%), and high content of free oil (mean 9.62 mg/g). It is important to acknowledge that this research does not account for movable water, as it is negligible; however, this factor should be taken into consideration when examining low-maturity shale formations.

4. Conclusions

This study elucidates the occurrence characteristics and determinants of pore fluids in shale oil reservoirs, including capillary-bound water, adsorbed oil, capillary-bound oil, and movable oil, and their interplays. The shale pore-fluid occurrence pattern has been delineated, with the following principal findings.

1) NMR T_1–T_2 provides an alternative and accurate technique for quantitatively analyzing pore fluids in shale oil reservoirs. Post-restoration of water and oil, the in-situ pore fluid content can be accurately assessed. Pore fluids are predominantly composed of capillary-bound water, with nearly half of it being depleted. Capillary-bound oil is the primary contributor to shale oil, succeeded by adsorbed and movable oil. Over one-third of the capillary-bound oil and nearly all movable oil are depleted. The characteristics of shale oil occurrence exhibit concurrent variations during pore-fluid depletion. Therefore, when restoring shale oil, not only should content correction be considered, but also changes in the occurrence state.
2) Shale oil contents tested by NMR T_1–T_2 agree well with those derived from Rock-Eval. Adsorbed oil obtained from T_1–T_2 spectra primarily refers to the oil adsorbed on pore surfaces and exhibits lower values compared to Rock-Eval measurements. NMR T_1–T_2 spectral free oil, a sum of capillary-bound and movable oil, aligns with Rock-Eval results. Correspondingly, the total oil from the T_1–T_2 spectra is generally lower than that determined by Rock-Eval. NMR T_1–T_2 is considered more suitable for detecting shale pore fluids, thereby enabling more accurate evaluation of shale oil reserves.
3) In shale oil reservoirs, capillary-bound water mainly occurs in micro- and minipores, coexisting with adsorbed oil and being significantly influenced by pore water. Capillary-bound oil is primarily found in mesopores, slightly constrained by pore water, while movable oil fills macropores. Consequently, mesopores and macropores are the primary repositories for free oil. Felsic-rich shales are conducive to the enrichment of shale oil, particularly free oil, due to the development of interparticle pores, lower BET SSA, and an abundance of mesopores and macropores.

CRediT authorship contribution statement

Jun-Hui Li: Methodology, Data curation, Conceptualization. **Fang-Ju Chen:** Methodology, Investigation, Data curation. **Jie Li:** Investigation. **Peng-Fei Zhang:** Writing – original draft, Methodology, Investigation. **Yan-Ping Zhu:** Methodology, Data curation. **Neng-Wu Zhou:** Methodology, Investigation, Funding acquisition. **Jia-Wei Hao:** Data curation. **Wei-Zheng Gao:** Investigation, Data curation. **Shuang-Fang Lu:** Writing – review & editing, Investigation.

Conflict of interest statement

The authors declare that they have no known competing financial interests or personal relationships that could have appeared to influence the work reported in this paper.

Acknowledgements

This study was financially supported by the National Natural Science Foundation of China (42572168) and the Sanya City Science and Technology Innovation Project (2022KJCX51).

References

Bai, J., Kang, Y., Chen, M., et al., 2020. Impact of surface chemistry and pore structure on water vapor adsorption behavior in gas shale. Chem. Eng. J. 402, 126238. https://doi.org/10.1016/j.cej.2020.126238.
Bai, L.H., Liu, B., Du, Y.J., et al., 2022. Distribution characteristics and oil mobility thresholds in lacustrine shale reservoir: Insights from N_2 adsorption experiments on samples prior to and following hydrocarbon extraction. Pet. Sci. 19 (2), 486–497. https://doi.org/10.1016/j.petsci.2021.10.018.
Bechtel, A., Jia, J., Strobl, S.A.I., et al., 2012. Palaeoenvironmental conditions during deposition of the Upper Cretaceous oil shale sequences in the Songliao Basin (NE China): Implications from geochemical analysis. Org. Geochem. 46, 76–95. https://doi.org/10.1016/j.orggeochem.2012.02.003.
Cao, Y., Jin, Z., Zhu, R., et al., 2023. Microstructures of continental organic-rich shale and its adjacent siltstone and carbonate rocks: An example from the Lucaogou Formation, Jimusar Sag, Junggar Basin, NW China. Geoenergy Sci. Eng. 225, 211705. https://doi.org/10.1016/j.geoen.2023.211705.
Cao, Y., Jin, Z., Zhu, R., et al., 2024. Comprehensive evaluation of the organic-rich saline lacustrine shale in the Lucaogou Formation, Jimusar Sag, Junggar Basin, NW China. Energy 294, 130786. https://doi.org/10.1016/j.energy.2024.130786.
Cheng, P., Xiao, X., Tian, H., et al., 2022. Differences in the distribution and occurrence phases of pore water in various nanopores of marine-terrestrial transitional shales in the Yangquan area of the northeast Qinshui Basin, China. Mar. Petrol. Geol. 137, 105510. https://doi.org/10.1016/j.marpetgeo.2021.105510.
Cheng, P., Xiao, X., Wang, X., et al., 2019. Evolution of water content in organic-rich shales with increasing maturity and its controlling factors: Implications from a pyrolysis experiment on a water-saturated shale core sample. Mar. Petrol. Geol. 109, 291–303. https://doi.org/10.1016/j.marpetgeo.2019.06.023.
D'Agostino, C., Mitchell, J., Mantle, M.D., et al., 2014. Interpretation of NMR relaxation as a tool for characterising the adsorption strength of liquids inside porous materials. Chem 20 (40), 13009–13015. https://doi.org/10.1002/chem.201403139.
Dang, W., Nie, H., Zhang, J., et al., 2022. Pore-scale mechanisms and characterization of light oil storage in shale nanopores: New method and insights. Geosci. Front. 13 (5), 101424. https://doi.org/10.1016/j.gsf.2022.101424.
Fang, C.H., Huang, Z.L., Wang, Q.Z., et al., 2014. Cause and significance of the ultra-low water saturation in gas-enriched shale reservoir. Nat. Gas Geosci. 25 (3), 471–476. https://doi.org/10.11764/j.issn.1672-1926.2014.03.0471 (in Chinese).
Fang, Z.X., Xiao, Q.S., Zhang, D.W., et al., 2023. Geological characteristics and exploration of continental fault-block shale oil reservoirs in the Subei Basin. Oil Gas Geol. 44 (6), 1468–1478. https://doi.org/10.11743/ogg20230611 (in Chinese).
Fleury, M., Romero-Sarmiento, M., 2016. Characterization of shales using T_1–T_2 NMR maps. J. Petrol. Sci. Eng. 137, 55–62. https://doi.org/10.1016/j.petrol.2015.11.006.
Gao, P., Xiao, X., Hu, D., et al., 2022. Water distribution in the ultra-deep shale of the Wufeng–Longmaxi Formations from the Sichuan Basin. Energies 15 (6), 2215. https://doi.org/10.3390/en15062215.
Gao, Z., Bai, L., Hu, Q., et al., 2024. Shale oil migration across multiple scales: A review of characterization methods and different patterns. Earth Sci. Rev. 254, 104819. https://doi.org/10.1016/j.earscirev.2024.104819.
Habina, I., Radzik, N., Topór, T., et al., 2017. Insight into oil and gas-shales compounds signatures in low field 1H NMR and its application in porosity evaluation. Microporous Mesoporous Mater. 252, 37–49. https://doi.org/10.1016/j.micromeso.2017.05.054.
Hu, T., Pang, X., Jiang, F., et al., 2021. Movable oil content evaluation of lacustrine organic-rich shales: Methods and a novel quantitative evaluation model. Earth Sci. Rev. 214, 103545. https://doi.org/10.1016/j.earscirev.2021.103545.
Jarvie, D.M., 2012. Shale resource systems for oil and gas: Part 2 Shale-oil resource systems. In: Shale Reservoirs—Giant Resources for the 21st Century. AAPG Memoir 97, 89–199. https://doi.org/10.1306/13321447M973489.

Jia, C., Pang, X., Song, Y., 2024. Basic principles of the whole petroleum system. Petrol. Explor. Dev. 51 (4), 780–794. https://doi.org/10.1016/S1876-3804(24)60506-9.
Jiang, Q.G., Li, M.W., Qian, M.H., et al., 2016. Quantitative characterization of shale oil in different occurrence states and its application. Petrol. Geol. Exp. 38 (6), 842–849. https://doi.org/10.11781/sysydz201606842 (in Chinese).
Jiang, X., Zhou, N., Li, B., et al., 2026. Organic-rich shale lithofacies classification scheme: Application and discussion. Nat. Resour. Res. 35 (1), 397–417. https://doi.org/10.1007/s11053-025-10545-3.
Jin, Z., Liang, X., Bai, Z., 2022. Exploration breakthrough and its significance of Gulong lacustrine shale oil in the Songliao Basin, Northeastern China. Energy Geosci 3 (2), 120–125. https://doi.org/10.1016/j.engeos.2022.01.005.
Li, J., Huang, W., Lu, S., et al., 2018b. Nuclear magnetic resonance T_1–T_2 map division method for hydrogen-bearing components in continental shale. Energy Fuel. 32 (9), 9043–9054. https://doi.org/10.1021/acs.energyfuels.8b01541.
Li, J., Jiang, C., Wang, M., et al., 2022a. Determination of in situ hydrocarbon contents in shale oil plays. Part 1: is routine Rock–Eval analysis reliable for quantifying the hydrocarbon contents of preserved shale cores? Org. Geochem. 170, 104449. https://doi.org/10.1016/j.orggeochem.2022.104449.
Li, J., Lu, S., Cai, J., et al., 2018a. Adsorbed and free oil in lacustrine nanoporous shale: a theoretical model and a case study. Energy Fuel. 32 (12), 12247–12258. https://doi.org/10.1021/acs.energyfuels.8b02953.
Li, J., Lu, S., Xie, L., et al., 2017. Modeling of hydrocarbon adsorption on continental oil shale: A case study on *n*-alkane. Fuel 206, 603–613. https://doi.org/10.1016/j.fuel.2017.06.017.
Li, J., Wang, M., Fei, J., et al., 2022b. Determination of in situ hydrocarbon contents in shale oil plays. Part 2: Two-dimensional nuclear magnetic resonance (2D NMR) as a potential approach to characterize preserved cores. Mar. Petrol. Geol. 145, 105890. https://doi.org/10.1016/j.marpetgeo.2022.105890.
Li, J., Wang, Y., Song, Z., et al., 2024b. Mobility of connate pore water in gas shales: A quantitative evaluation on the Longmaxi shales in the southern Sichuan Basin. China. Mar. Petrol. Geol. 161, 106674. https://doi.org/10.1016/j.marpetgeo.2023.106674.
Li, W., Wang, J., Jia, C., et al., 2024a. Carbon isotope fractionation during methane transport through tight sedimentary rocks: phenomena, mechanisms, characterization, and implications. Geosci. Front. 15 (6), 101912. https://doi.org/10.1016/j.gsf.2024.101912.
Li, Y., Chen, G., Cai, Z., et al., 2024c. Occurrence of methane in organic pores with surrounding free water: a molecular simulation study. Chem. Eng. J. 497, 155597. https://doi.org/10.1016/j.cej.2024.155597.
Liu, B., Jiang, X.W., Bai, L.H., et al., 2022b. Investigation of oil and water migrations in lacustrine oil shales using 20 MHz 2D NMR relaxometry techniques. Pet. Sci. 19 (3), 1007–1018. https://doi.org/10.1016/j.petsci.2021.10.011.
Liu, B., Shi, J., Fu, X., et al., 2018. Petrological characteristics and shale oil enrichment of lacustrine fine-grained sedimentary system: A case study of organic-rich shale in first member of Cretaceous Qingshankou Formation in Gulong Sag, Songliao Basin, NE China. Petrol. Explor. Dev. 45 (5), 884–894. https://doi.org/10.1016/S1876-3804(18)30091-0.
Liu, H.M., Li, J.L., Liu, P., et al., 2022a. Enrichment conditions and strategic exploration direction of Paleogene shale oil in Jiyang depression. Acta Pet. Sin. 43 (12), 1717–1729. https://doi.org/10.7623/syxb202212004 (in Chinese).
Ma, L., Yu, Q., 2022. Experimental investigation into simultaneous adsorption of water vapor and methane onto shales. J. Hydrol. 604, 127200. https://doi.org/10.1016/j.jhydrol.2021.127200.
Ma, W., Li, J., Wang, M., 2024. Determination of in situ hydrocarbon contents in shale oil plays: Part 3: Quantification of light hydrocarbon evaporative loss in old cores based on preserved shales. Mar. Petrol. Geol. 160, 106574. https://doi.org/10.1016/j.marpetgeo.2023.106574.
Su, S., Jiang, Z., Shan, X., et al., 2018. The effects of shale pore structure and mineral components on shale oil accumulation in the Zhanhua Sag, Jiyang Depression, Bohai Bay Basin, China. J. Petrol. Sci. Eng. 165, 365–374. https://doi.org/10.1016/j.petrol.2018.02.030.
Su, S., Jiang, Z., Shan, X., et al., 2019. Effect of lithofacies on shale reservoir a nd hydrocarbon bearing capacity in the Shahejie Formation, Zhanhua Sag, eastern China. J. Petrol. Sci. Eng. 174, 1303–1308. https://doi.org/10.1016/j.petrol.2018.11.048.
Sun, L.D., Jia, C.Z., Zhang, J.F., et al., 2024a. Resource potential of Gulong shale oil in the key areas of Songliao Basin. Acta Petrol. Sin 45 (12), 1699–1714. https://link.cnki.net/urlid/11.2128.TE.20241210.1528.002.
Sun, L.D., Zhu, R.K., Zhang, T.S., et al., 2024b. Advances and trends of non-marine shale sedimentology: a case study from Gulong Shale, Songliao Basin, NE China. Petrol. Explor. Dev. 51 (6), 1183–1198. https://doi.org/10.11698/PED.20240258 (in Chinese).
Tian, H., He, K., Huangfu, Y., et al., 2024. Oil content and mobility in a shale reservoir in Songliao Basin, Northeast China: Insights from combined solvent extraction and NMR methods. Fuel 357, 129678. https://doi.org/10.1016/j.fuel.2023.129678.
Tian, S., Erastova, V., Lu, S., et al., 2018. Understanding model crude oil component interactions on kaolinite silicate and aluminol surfaces: Toward improved understanding of shale oil recovery. Energy Fuel. 32 (2), 1155–1165. https://doi.org/10.1021/acs.energyfuels.7b02763.
Wang, J., Chen, F.W., Li, W.B., et al., 2025a. A multi-scale and multi-mechanism coupled model for carbon isotope fractionation of methane during shale gas production. Petrol. Sci. 22 (7), 2719–2746. https://doi.org/10.1016/j.petsci.2025.03.034.
Wang, J., Lu, S., Zhang, P., et al., 2024. Characterization of shale oil and water micro-occurrence based on a novel method for fluid identification by NMR T_2 spectrum. Fuel 374, 132426. https://doi.org/10.1016/j.fuel.2024.132426.
Wang, J.J., Zhang, P.F., Lu, S.F., et al., 2025c. Insights into microscopic oil occurrence characteristics in shales from the Paleogene Funing Formation in Subei Basin, China. Pet. Sci. 22 (1), 55–75. https://doi.org/10.1016/j.petsci.2024.07.025.
Wang, L., Zhang, Y.F., Zou, R., et al., 2025b. Applications of molecular dynamics simulation in studying shale oil reservoirs at the nanoscale: advances, challenges and perspectives. Pet. Sci. 22 (1), 234–254. https://doi.org/10.1016/j.petsci.2024.09.023.
Wang, M., Li, M., Li, J.B., et al., 2022a. The key parameter of shale oil resource evaluation: oil content. Pet. Sci. 19 (4), 1443–1459. https://doi.org/10.1016/j.petsci.2022.03.006.
Wang, M., Ma, R., Li, J., et al., 2019. Occurrence mechanism of lacustrine shale oil in the Paleogene Shahejie Formation of Jiyang Depression, Bohai Bay Basin, China. Petrol. Explor. Dev. 46 (4), 833–846. https://doi.org/10.1016/S1876-3804(19)60242-9.
Wang, M., Xue, H., Tian, S., et al., 2015. Fractal characteristics of Upper Cretaceous lacustrine shale from the Songliao Basin, NE China. Mar. Petrol. Geol. 67, 144–153. https://doi.org/10.1016/j.marpetgeo.2015.05.011.
Wang, X., Wang, M., Li, J., et al., 2022b. Thermal maturity: the controlling factor of wettability, pore structure, and oil content in the lacustrine Qingshankou shale, Songliao Basin. J. Petrol. Sci. Eng. 215, 110618. https://doi.org/10.1016/j.petrol.2022.110618.
Wang, Y., Li, P., Feng, Z., et al., 2023. Geochemical characteristics of shales from the first member of Qingshankou Formation in Gulong Sag, Songliao Basin, China: Implication for mechanism of organic matter enrichment. Mar. Petrol. Geol. 150, 106142. https://doi.org/10.1016/j.marpetgeo.2023.106142.
Wu, H., Xu, H., Zhou, H., et al., 2024. Astronomical control on organic matter enrichment of lacustrine mudstones in the first member of the Late Cretaceous Qingshankou Formation, the Songliao Basin, NE China. J. Asian Earth Sci. 259, 105906. https://doi.org/10.1016/j.jseaes.2023.105906.
Xiang, X., Dan, W., Lu, S., et al., 2024. Insight into fluid occurrence and pore structure of lacustrine shale from the Cretaceous Tengger Formation, A'nan Sag, Erlian Basin, China. Energy Fuel. 38 (14), 12960–12977. https://doi.org/10.1021/acs.energyfuels.4c02071.
Xu, Y., Lun, Z., Pan, Z., et al., 2022. Occurrence space and state of shale oil: A review. J. Petrol. Sci. Eng. 211, 110183. https://doi.org/10.1016/j.petrol.2022.110183.
Xue, H., Ding, G., Dong, Z., et al., 2022. Study on the wettability and spontaneous imbibition characteristics of lacustrine shale. Geofluids 2022, 4023435. https://doi.org/10.1155/2022/4023435.
Xue, H.T., Tian, S.S., Wang, W.M., et al., 2016. Correction of oil content: One key parameter in shale oil resource assessment. Oil Gas Geol. 37 (1), 15–22. https://doi.org/10.11743/ogg20160103 (in Chinese).
Yang, Y., Liu, J., Yao, J., et al., 2020. Adsorption behaviors of shale oil in kerogen slit by molecular simulation. Chem. Eng. J. 387, 124054. https://doi.org/10.1016/j.cej.2020.124054.
Zhang, H., Huang, H., Li, Z., et al., 2019a. Oil physical status in lacustrine shale reservoirs—A case study on Eocene Shahejie Formation shales, Dongying Depression, East China. Fuel 257, 116027. https://doi.org/10.1016/j.fuel.2019.116027.
Zhang, J.Y., Zhu, R.K., Wu, S.T., et al., 2023c. Microscopic oil occurrence in high-maturity lacustrine shales: Qingshankou Formation, Gulong Sag, Songliao Basin. Pet. Sci. 20 (5), 2726–2746. https://doi.org/10.1016/j.petsci.2023.08.026.
Zhang, P., Lu, S., Li, J., 2019b. Characterization of pore size distributions of shale oil reservoirs: A case study from Dongying sag, Bohai Bay Basin. China. Mar. Petrol. Geol. 100, 297–308. https://doi.org/10.1016/j.marpetgeo.2018.11.024.
Zhang, P., Lu, S., Li, J., et al., 2017. Characterization of shale pore system: A case study of Paleogene Xin'gouzui Formation in the Jianghan Basin. China. Mar. Petrol. Geol. 79, 321–334. https://doi.org/10.1016/j.marpetgeo.2016.10.014.
Zhang, P., Lu, S., Li, J., et al., 2022a. Evaluating microdistribution of adsorbed and free oil in a lacustrine shale using nuclear magnetic resonance: a theoretical and experimental study. J. Petrol. Sci. Eng. 212, 110208. https://doi.org/10.1016/j.petrol.2022.110208.
Zhang, P., Lu, S., Li, J., et al., 2023b. Oil occurrence mechanism in nanoporous shales: a theoretical and experimental study. Mar. Petrol. Geol. 156, 106422. https://doi.org/10.1016/j.marpetgeo.2023.106422.
Zhang, P., Lu, S., Lin, Z., et al., 2022b. Key oil content parameter correction of shale oil resources: a case study of the Paleogene Funing Formation, Subei Basin, China. Energy Fuel. 36 (10), 5316–5326. https://doi.org/10.1021/acs.energyfuels.2c00610.
Zhang, P., Wu, H., Lu, S., et al., 2024a. The occurrence of pore fluid in shale-oil reservoirs using nuclear magnetic resonance: the Paleogene funing Formation, Subei Basin, Eastern China. Mar. Petrol. Geol. 167, 106986. https://doi.org/10.1016/j.marpetgeo.2024.106986.
Zhang, P.F., Lu, S.F., Wang, J.J., et al., 2024b. Microscopic occurrence and distribution of oil and water in situ shale: evidence from nuclear magnetic resonance. Pet. Sci. 21 (6), 3675–3691. https://doi.org/10.1016/j.petsci.2024.04.007.
Zhang, S., Zhang, B., Wang, X., et al., 2023a. Gulong shale oil enrichment mechanism and orderly distribution of conventional–unconventional oils in the Cretaceous Qingshankou Formation, Songliao Basin, NE China. Petrol. Explor. Dev. 50 (5), 1045–1059. https://doi.org/10.1016/S1876-3804(23)60448-3.
Zhao, W., Bian, C., Li, Y., et al., 2023b. Enrichment factors of movable hydrocarbons in lacustrine shale oil and exploration potential of shale oil in Gulong Sag, Songliao Basin, NE China. Petrol. Explor. Dev. 50 (3), 520–533. https://doi.org/10.1016/S1876-3804(23)60407-0.

Zhao, W., Bian, C., Li, Y., et al., 2024. "Component flow" conditions and its effects on enhancing production of continental medium-to-high maturity shale oil. Petrol. Explor. Dev. 51 (4), 826–838. https://doi.org/10.1016/S1876-3804(24)60509-4.

Zhao, W.Z., Zhu, R.K., Zhang, J.Y., et al., 2023a. Classification, exploration and development status and development trend of continental shale oil in China. China Petrol. Explore 28 (4), 1–13. https://doi.org/10.3969/j.issn.1672-7703.2023.04.001 (in Chinese).

Zhao, X.Z., Pu, X.G., Jin, F.M., et al., 2023c. Enrichment law and favorable exploration area of shale-type shale oil in Huanghua depression. Acta Pet. Sin. 44 (1), 158–175. https://doi.org/10.7623/syxb202301010 (in Chinese).

Zhu, X.Y., Duan, H.L., Sun, Y.X., 2023. Breakthrough and significance of Paleogene continental shale oil exploration in Gaoyou sag, Subei Basin. Acta Pet. Sin. 44 (8), 1206–1221. https://doi.org/10.7623/syxb202308002 (in Chinese).

Zolfaghari, A., Dehghanpour, H., Holyk, J., 2017a. Water sorption behaviour of gas shales: I. Role of clays. Int. J. Coal Geol. 179, 130–138. https://doi.org/10.1016/j.coal.2017.05.008.

Zolfaghari, A., Dehghanpour, H., Xu, M., 2017b. Water sorption behaviour of gas shales: II. Pore size distribution. Int. J. Coal Geol. 179, 187–195. https://doi.org/10.1016/j.coal.2017.05.009.